INVESITGATING EFFECTS OF SENSOR ARRANGEMENT AND HARDWARE CHANGES ON MEASURED RANGE-HOOD CAPTURE EFFICIENCY PERFORMANCE

A Thesis

by

EDGAR MICHAEL YOKUBAITIS

Submitted to the Office of Graduate and Professional Studies of
Texas A&M University
in partial fulfillment of the requirements for the degree of

MASTER OF SCIENCE

Chair of Committee,	Michael B. Pate
Committee Members,	Jorge Alvarado
	Dion Antao
Head of Department,	Andreas A. Polycarpou

May 2021

Major Subject: Mechanical Engineering

ABSTRACT

Kitchen range hoods remove contaminants released by cooking and are instrumental in maintaining acceptable indoor air qualities. Capture efficiency testing was developed to provide a unified metric describing the performance of a range hood based on its ability to remove contaminated air from the cooking space. The current testing standard set forth in ASTM-E3087 involves releasing an inert tracer gas into a test chamber that simulates a residential kitchen and then measuring the concentration of the tracer gas at three locations to include the air within the chamber, in the chamber exhaust ducting, and finally at the inlet to the chamber. The ASTM standard specifies that a single sensor must be used for all three concentration measurements.

This research study investigates two alternate testing methods that are both based on using an array of three concentration sensors to perform those measurements necessary for determining capture efficiency. The first method requires manual data entry for each concentration measurement for ten test points. The second method involves automated recording of approximately one thousand test points. Both proposed methods intend to reduce potential operator error in the test, thereby reducing uncertainty of capture efficiency measurements.

A series of validation tests showed with 95% confidence that both proposed multi-sensor methods produce results that are statistically similar to those gathered using the standard

method outlined in ASTM-E3087. On average, the manual-method results differed from the standard method by 1.502% while automatic results differed by 1.516%. Repeatability of each multi-sensor method was then assessed by comparing the standard deviations of tests performed with both methods. The manual method reported results with standard deviations of 1.573% on average, compared to 1.769% for the automatic method. This suggests the automatic method is less repeatable, likely due to it lacking a means to filter outlier measurements.

Finally, an additional study made use of the manual multi-sensor method to test the impacts of test chamber hardware layouts. This investigation showed that moving the tracer emitters two inches further from a sample range hood resulted in an 18% percent reduction in measured capture efficiency at the low-speed setting.

ACKNOWLEDGEMENTS

I would like to thank my committee chair, Dr. Pate, and my committee members, Dr. Antao, and Dr. Alvarado, for their guidance and support throughout the course of this research.

Thanks also go to my friends and colleagues at the RELLIS Energy Efficiency Laboratory as well as the Mechanical Engineering department faculty and staff for making my time at Texas A&M University a great experience.

Finally, thanks to my mother and father for their constant support and encouragement.

CONTRIBUTORS AND FUNDING SOURCES

Contributors

This work was supervised by a thesis committee consisting of Dr. Michael Pate and Dr. Dion Antao of the Department of Mechanical Engineering and Dr. Jorge Alvarado of the Department of Engineering Technology and Industrial Distribution.

Funding Sources

Graduate study was supported by a Graduate Research Assistantship from Texas A&M University.

NOMENCLATURE

ASTM	American Society for Testing and Materials
HVI	The Home Ventilating Institute
CO2	Carbon Dioxide
P	Pressure (general)
P_D	Chamber Depressurization
P_V	Venturi Pressure
C_I	Concentration of CO2 at chamber inlet
C_C	Concentration of CO2 inside chamber
C_E	Concentration of CO2 in chamber exhaust
C	Duct Discharge Coefficient
ε	Duct Expansibility Factor
D	Duct Diameter
d	Venturi Tube Throat Diameter
β	Diameter Ratio
ρ	Density of Air within Test Chamber
ρ_1	Density of Air within Venturi Tube
Q_V	Mass flow rate of air through venturi tube
Q	Volumetric flow rate of air leaving test chamber
Q_C	Corrected volumetric flow rate of air leaving test chamber.
IR_{max}	Maximum allowable injection rate of CO2

V	Volume of test chamber
t_{ss}	Estimated time required to achieve steady state.
AVG	Average
SDEV	Sample standard deviation
COV	Coefficient of Variance
δ_{SE}	Standard error
δ_{P}	Precision uncertainty
δ	Overall uncertainty
t	Calculated t-value used in hypothesis testing
μ_A	Mean value of a given group.
n	Number of elements in a given group.
Cfm	Cubic feet per minute – measure of volumetric flow rate
Lpm	liters per minute – measure of volumetric flow rate
i.w.c.	Inches of Water Column – measure of pressure
T	Temperature
CE	Capture Efficiency
REEL	Riverside Energy Efficiency Lab/ RELLIS Energy Efficiency Lab

TABLE OF CONTENTS

Page

LIST OF FIGURES

Page

LIST OF TABLES

Page

CHAPTER 1.

INTRODUCTION

Cooking is a necessary part of most people's lives, and many people enjoy it as a hobby or occupation. However, the cooking process releases a myriad of contaminants into the air, decreasing indoor air quality (1). To mitigate this issue, most kitchens contain some form of range hood to remove contaminated air before it can mix with the surroundings. Not all range hoods are made equal; some hoods outperform others in terms of flow rate, energy efficiency, cost, etc. As a result, there are often tradeoffs to consider when selecting an appropriate range hood for a given space. Standardized performance testing and rating systems simplify the comparison process and help reduce confusion in marketing. Many factors beyond just flow rate contribute to a fan's ability to maintain good indoor air quality, so airflow testing to establish flow rates alone is insufficient for assessing a range hood's effectiveness, therefore capture efficiency (CE) testing was developed to provide a single metric by which a kitchen range hood's ability to remove contaminants might be assessed.

ASTM-E3087 outlines the standardized testing procedure for measuring CE of kitchen range hoods. The general process as outlined in this standard is to use an inert tracer gas (e.g. CO_2) to track the plume of air emitted from a simulated kitchen range by measuring the concentration of the tracer in the test chamber, the exhaust ducting, and in the ambient air inlet of the test chamber (2). Figure 1.1 depicts a schematic the testing chamber used for range hood capture efficiency (RHCE) testing at REEL from a top-down perspective, noting the dimensions and relative locations of relevant pieces of

equipment. Figure 1.2 depicts the same chamber from a side perspective to show relative elevations of equipment and sampling points (3).

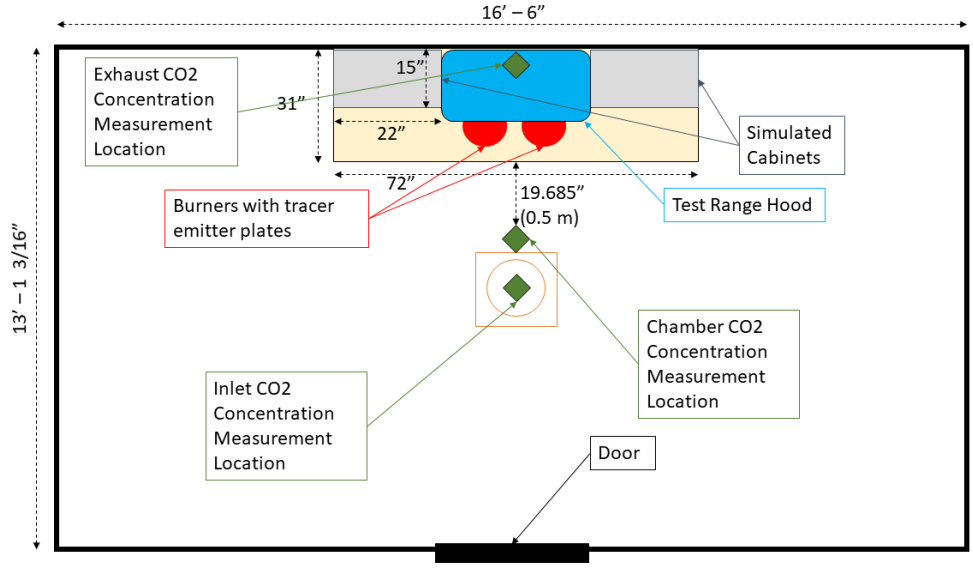

Figure 1.1: A top-down schematic of the RHCE testing chamber at REEL that meets the guidelines set forth in ASTM-E3087.

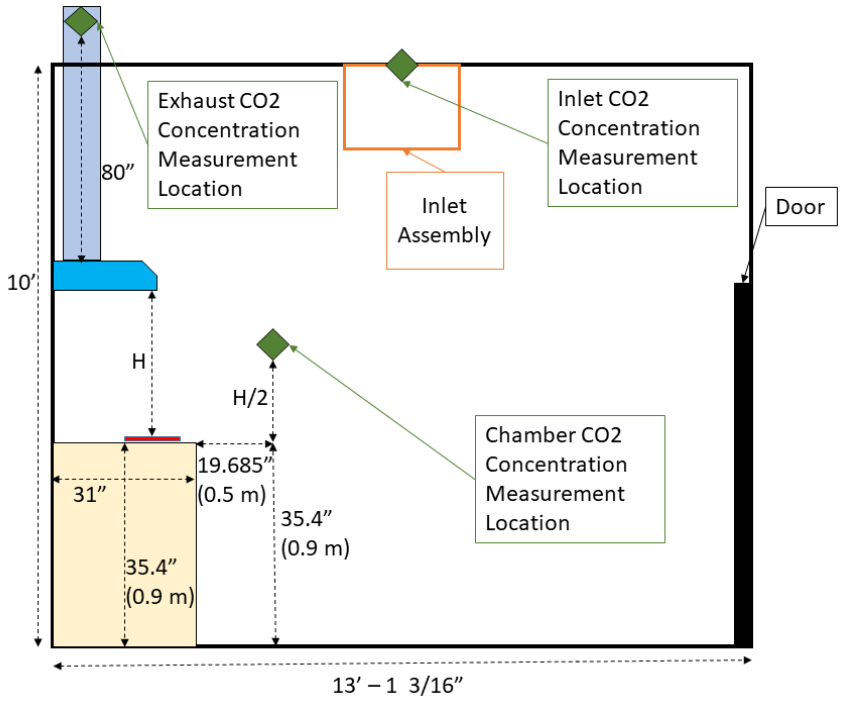

Figure 1.2: Side profile schematic of the RHCE testing chamber at REEL.

By taking measurements at these three locations denoted in Figures 1.1 and 1.2, the CE of the range hood can be calculated as shown in equation 1.

$$CE = \frac{C_{exhaust} - C_{chamber}}{C_{exhaust} - C_{inlet}} \quad [1]$$

Carbon Dioxide is commonly used as the tracer gas due to its availability as well as the abundance of CO2 measurement devices. The tracer is released into the chamber until an approximate steady state has been achieved. The test procedure defines this as occurring after at least four full air changes have occurred within the chamber (2). When steady state has been achieved, the technician can begin to record data.

ASTM-E3087 states that only one CO2 concentration sensor may be used during a test (2). To satisfy this, the existing test station at REEL uses a single SBA-5 CO2 sensor developed by PP Systems. The sensor is connected to an actuator that allows the technician to toggle between the inlet, chamber, and exhaust measurement points.

There are several advantages to using a single sensor. Even excluding the base cost of additional instruments, it is much cheaper to maintain the calibration of a single device than an array of devices. In addition, using a single sensor simplifies the process of accounting for error and uncertainty in the overall capture efficiency measurement. Despite these advantages, this method comes with its own drawbacks. While the physical toggling between measurement tap locations is quick, the duration of the test is lengthened by of the accumulated time spent waiting for measurements to stabilize, as a result of the long length of the sample line running from the CO2 sensor and actuator to the sample points. This seemingly minor issue can become compounded in cases where there are potentially orders of magnitude differences among the concentrations of tracer gas at the different measurement locations. This standard approach also introduces the possibility of human bias, as the technician is left to decide when a point is sufficiently stable after switching measurement positions. When only a single sensor is used for measurement, the tracer concentration can only be measured at one location at any given time. As a result, the measurements cannot be viewed as a continuous stream but as several distinct points that can potentially occur several minutes apart from each other. The additional context provided by a continuous stream of measurements allows the

technician to distinguish more easily between random fluctuations and gross changes that could indicate instability or other potential problems.

The aim of this study is to suggest and validate the accuracy of a multi-sensor testing system as a potential improvement and alternative to the range-hood testing procedures described in ASTM-E3087. Furthermore, this study could lead to improvements in test accuracy and repeatability, while making a substantial step towards potential automation of the test.

CHAPTER 2.

ADAPTING EXISTING TESTING SYSTEMS FOR MULTI-SENSOR TESTING

The capture efficiency testing software used by technicians at REEL was initially designed for use with a single CO2 concentration measurement device. A single SBA-5 CO2 gas analyzer calibrated for a 0-15,000 ppm measurement range was used, requiring technicians to manually toggle between three measurement tap lines. Before multi-sensor testing procedures could be developed or validated, the data collection system required substantial modification.

In modifying the LabVIEW virtual instrument, three major items needed to be addressed: 1.) interfacing between the computer and the additional concentration sensors, 2.) additional instantaneous calculations and real time data displays, and 3.) assurance of sensor accuracy. Each of these three items are discussed in the following sections.

2.1. Measurement Device Interfacing and Range Selection

The existing single sensor LabVIEW virtual instrument used at REEL interfaces over USB with a National Instruments cDAQ-9174 chassis equipped with an NI 9205 analog voltage input module and an NI 9211 thermocouple input module. The voltage input module can accept up to 16 differential analog inputs in a 0-10-volt range. The previous setup only used three of these channels, leaving several available ports for the two additional inputs. To accommodate the new multi-sensor approaches, two additional SBA-5 analyzers were connected to this input module, one calibrated in a 0-

1,000 ppm range and the other in a 0-10,000 ppm range. Table 2.1 summarizes the ranges, serial numbers, and placement of the three SBA-5 analyzers.

Table 2.1: Summary of the locations and detection ranges of the three CO2 sensors installed.

Location	Serial Number	Range	Device Accuracy	Notes
Inlet	SBA5-5939	0-1,000 ppm	< 10 ppm	New sensor
Chamber	SBA5-5940	0-10,000 ppm	< 100 ppm	New sensor
Exhaust	SBA5-5297	0-15,000 ppm	< 150 ppm	The analyzer used by REEL for single sensor CE testing

The new 1,000-ppm sensor was put in place to measure the inlet concentration of CO2 as this concentration is rarely greater than 600 ppm during testing. The new 10,000-ppm sensor was placed to measure the concentration of CO2 within the chamber. The chamber concentration only comes close to the limits of this range in extreme experimental cases, and the range can be adjusted in the device's settings in the future, if necessary. Finally, the original SBA-5 unit was connected to measure the exhaust concentration of CO2. This analyzer was scaled for a range of 0-15,000-ppm, well above the exhaust concentration seen in normal testing. The wide range settings on both the chamber and exhaust sensors were needed for other capture efficiency experiments being performed during the development of the three-sensor measurement apparatus, but in the future these ranges should be reduced to preserve accuracy and resolution.

2.2. Internal Calculations and Displays

With the sensors assigned and connected to physical channels on the DAQ's analogue input module, the next step in development was to add several internal calculations and real-time displays within the virtual instrument. Figure 2.1 shows the user interface for the updated three-sensor input virtual instrument. When in operation, the virtual instrument polls the DAQ 100 samples at a rate of 100 Hz. This updates the current displayed value for each measurement once per second with the average of the collected samples. The raw data stream from the DAQ is split into the respective measurements and converted into the appropriate units before being passed through to the graph displays. At this step, the CO2 concentrations are used to calculate an instantaneous CE measurement that is both recorded in the raw data output file and plotted over time to help visualize potential fluctuations over the course of the test. Each data element is then passed through to the next loop iteration with a shift register.

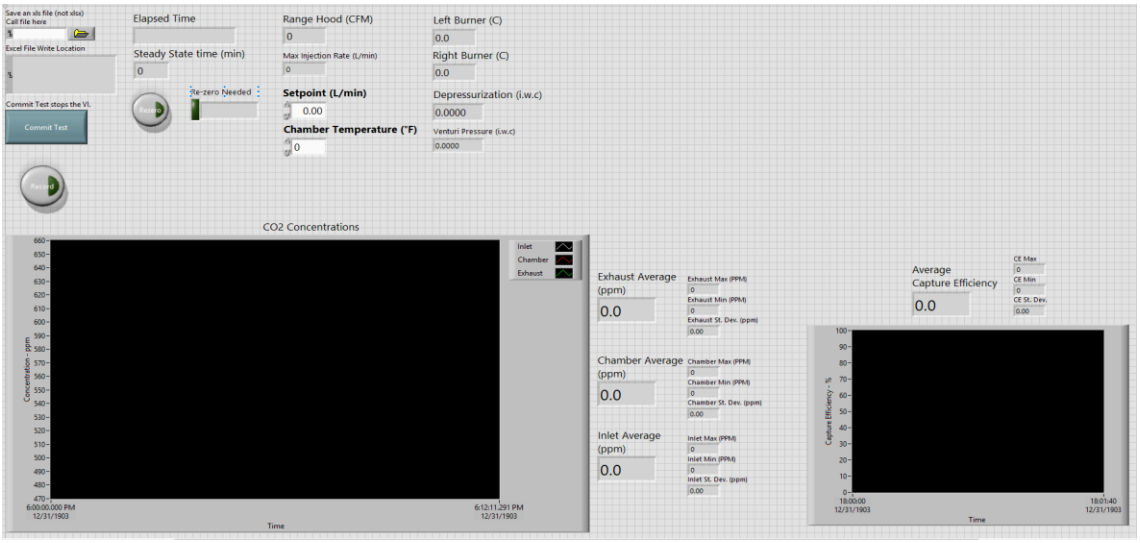

Figure 2.1: LabVIEW virtual instrument interfaces for the three-sensor testing format.

The virtual instrument then groups the current set of measurements with the previous nine sets before displaying an average of the ten most recent points for each parameter. The standard deviation as well as the maximum and minimum values are displayed alongside the average for the three concentration measurements as well as the calculated capture efficiency. The displayed data set is then appended to a raw data output file with a date and time code. These raw results can be accessed upon completion of the test. Examples of the intermediate calculations performed by the virtual instrument are provided in Chapter 3.

2.3. Ensuring Sensor Accuracy

The final concern in adapting the existing virtual instrument for multi-sensor testing is ensuring the accuracy of measurements from all three sensors. In the existing test procedure, this accuracy assurance is done through the frequent re-zeroing of the

instrument. By default, each of the SBA-5 sensors is set up to automatically perform a twenty-five second zeroing operation every twenty minutes. This step ensures that measurements do not drift over time, thereby maintaining accuracy. If re-zeroing occurs during a single sensor test, the technician is required to wait until the operation finishes before resuming data collection. While it might be slightly inconvenient, the auto-zeroing does not present any problems in tests where measurements are taken manually. Specifically, a human technician can easily identify when zeroing has begun and disregard the CO2 concentration reported by the sensor during these intervals. However, even with a single device these intervals present a major challenge in the development of any form of automated system. The issue is exacerbated when three sensors are used as there is a possibility of the auto-zeroing intervals of the three sensors coming out of sync. To avoid this potential problem, while still retaining its accuracy benefits, the automatic re-zeroing function was deactivated on each device and replaced by a single command button within the virtual instrument.

First, each of the devices was connected to the CE station computer via a USB connection to allow control from the virtual instrument. The SBA-5 sensors do not currently have any LabVIEW drivers available, but they can be controlled using simple ASCII string commands (4). To replace the automatic zeroing process, a control was added to send the re-zero command to all three analyzers simultaneously when the single command button on the virtual instrument interface is pressed.

Pressing the re-zero command button also resets a timer that indicates how long it has been since the last re-zero and alerts the technician with an indicator light if more

than twenty minutes have passed since the last re-zeroing. In practice this procedure allows the technician to re-zero the sensors after steady state has been achieved, to wait until the operation completes, and then to begin recording data. If a test proceeds for more than 20 minutes, the technician can pause the data recording, run the re-zero command, and then resume data recording after the readings stabilize.

CHAPTER 3.

INTERMEDIATE TEST CALCULATIONS

3.1. Converting Raw Signals to Usable Data

The data input to LabVIEW is in the form of voltage measurements made by the DAQ system. This data by itself is meaningless and needs to be converted to the units of the parameters it represents. Because all the sensors used have linear calibration curves, the conversions are simply multiplication by the appropriate scaling factor and adding the appropriate offset. These two values are determined by performing a linear curve-fit to data collected during device calibration. The three CO2 concentration sensors output in different measurement ranges, namely 0-1,000 ppm for the inlet, 0-10,000 ppm for the chamber, and 0-15,000 ppm for the exhaust. Therefore, their scaling factors are different from each other. A set of raw voltage measurements is presented in Table 3.1 for subsequent sample calculations.

Table 3.1: Example of Raw Sensor Data

Parameter	**Symbol**	**Units**	**Value**	**Scaling Factor**	**Offset**
Depressurization	P_D*	V	0.8576	0.3125	-0.25
Venturi Pressure	P_V*	V	1.4814	0.9376	-0.75
Inlet CO2 Concentration	C_I*	V	2.2055	200	0

Table 3.1 Continued

Parameter	Symbol	Units	Value	Scaling Factor	Offset
Chamber CO2 Concentration	C_C*	V	0.3566	2000	0
Exhaust CO2 Concentration	C_E*	V	1.8093	3000	0

All these raw voltages are converted by a formula of the same form, so only the first will be explicitly calculated; all others are presented in Table 3.2:

$$P_D = (P_D^* * 0.3125) + (-0.25)$$

$$P_D = (0.8576 * 0.3125) - 0.25$$

$$P_D = 0.018\ [iwc]$$

Table 3.2: Example of Converted Sensor Data

Parameter	Symbol	Units	Value
Depressurization	P_D	i.w.c*[1]	0.018
Venturi Pressure	P_V	i.w.c*[1]	0.639
Inlet CO2 Concentration	C_I	ppm	441.1
Chamber CO2 Concentration	C_C	ppm	713.2
Exhaust CO2 Concentration	C_E	ppm	5427.9

[1] i.w.c. – Inches of water column. A measure of pressure in reference to that exerted by a 1-inch-high column of water. 1 i.w.c. is equal to approximately 249 Pascals, or about 0.036 pounds per square inch. This unit of measure is used due to the relatively low pressure differentials that are exerted by a range hood during testing.

3.2. Calculating Fan Flow Rate

First, several fixed parameters must be defined. For examples, the discharge coefficient, expansibility factor, duct diameter, Venturi throat diameter, as well as the Venturi tube diameter are all taken to be input constants, but the Chamber air density is determined by using a lookup-table based on the chamber temperature input by the technician. These additional constants and parameters are organized in Table 4.3.

Table 3.3: Additional Parameters for Flow Rate Calculations

Parameter	**Symbol**	**Units**	**Value**
Discharge Coefficient	C	--	0.995
Expansibility Factor	ε	--	0.988
Duct Diameter	D	inches	8
Venturi Throat Diameter	d	Inches (m)	4 (0.1016)
Chamber Air Density	ρ	kg/m^3	1.1861
Venturi Tube Air Density	ρ_1	kg/m^3	1.225

The diameter ratio of the venturi tube can then be calculated as the ratio of the throat diameter to the input duct diameter:

$$\beta = \frac{d}{D} = \frac{4\ [in.]}{8\ [in.]} = 0.5$$

Next, the mass flow rate of air through the venturi tube must be calculated:

$$Q_V = \frac{C}{\sqrt{1-\beta^4}} * \varepsilon * \frac{\pi}{4} * d^2 * \sqrt{2 * P_V * \rho_1}$$

$$Q_V = \frac{(0.995)}{\sqrt{1-(0.5)^4}}(0.988)\frac{\pi}{4}(0.1016\,[m])^2\sqrt{2\left(0.639\,[iwc] * 249.0889\,\frac{[Pa]}{[iwc]}\right) * 1.225[kg/m^3]}$$

$$Q_V = 0.162548\,[kg/s]$$

The mass flow rate of air through the venturi tube can then be used to find the find the volumetric flow rate of air leaving the test chamber:

$$Q = \frac{Q_V}{\rho}$$

$$Q = \frac{0.162548\,[\frac{kg}{s}]}{1.1861\,[\frac{kg}{m^3}]}$$

$$Q = 0.137044\,[\frac{m^3}{s}]$$

This volume flow rate can then be converted into cubic feet per minute as follows:

$$Q = 0.137044\,\left[\frac{m^3}{s}\right] * \left(\frac{3.28084\,[ft]}{1[m]}\right)^3 * \frac{60\,[s]}{1\,[min]}$$

$$Q = 290.38\,[cfm]$$

This flow rate must then be scaled using calibration factors specific to the Venturi tube in use:

$$Q_C = 1.1142 * Q - 6.8037$$

$$Q_C = 1.1142 * 290.38 - 6.8037$$

$$Q_C = 316.738\,[cfm]$$

3.3. Determining Tracer Gas Injection Rate

Now that the flow rate of air out of the chamber has been calculated, the maximum allowable tracer gas injection rate as well as the estimated steady-state time can be calculated. The maximum tracer gas injection rate is defined as one half of one percent of the rate of exhausted airflow:

$$IR_{max} = 0.005 * Q_C$$

$$IR_{max} = 0.005 * 316.738\ [cfm]$$

$$IR_{max} = 1.58369\ [cfm]$$

The mass flow controller used for testing requires inputs in the units of liters per minute, so the injection rate units need to be converted:

$$IR_{max} = 1.4519\ [cfm] * \frac{28.3168\ [l]}{1\ [m^3]}$$

$$IR_{max} = 44.845\ [lpm]$$

In practice, technicians at REEL select the injection rate for a test by rounding the maximum rate allowable down to the nearest multiple of five liters per minute. This practice is intended to quickly select an injection rate that is less than the calculated maximum, while still being high enough to ensure that the difference in CO_2 concentration between the chamber exhaust and inlet is at least 100 times greater than the stated accuracy of the concentration sensor used. This lower-bounding condition for acceptable tracer gas injection rates is specified in Section 8.5 of ASTM-E3087 (2). In cases where the maximum injection rate is calculated to be either exactly a multiple of five or within one half above a multiple of five, the technician may choose the next

lowest multiple of five liters per minute as the injection rate for the test. For example, in the above calculated example, the maximum allowable injection rate of 44.845 lpm would be rounded down to a selected value of 40 lpm. If the maximum injection rate were calculated to be as high as 45.5, the rounded value of 40 lpm would still be selected. However, if the maximum injection rate were calculated to be 45.6 lpm or more, the selected rate for the test would be rounded to 45 lpm. This additional allowance for rounding down at technician discretion is meant to allow the technician to account for random fluctuations and uncertainties in the flow rate of air through the range hood, and it is necessary due to the flow rate's impact on the maximum allowable injection rate.

3.4. Estimating Steady State Time

The steady-state time for a capture efficiency test is estimated as the time required for four full air changes within the test chamber. The internal volume of the capture efficiency testing chamber at REEL is known to be 2063.1 cubic feet. Knowing this value and the rate of exhaust from the chamber calculated above, an estimate for the steady state time can be calculated:

$$t_{ss} = 4 * \frac{V}{Q_C}$$

$$t_{ss} = 4 * \frac{2063.1\ [ft^3]}{316.738\ [\frac{ft^3}{min}]}$$

$$t_{ss} = 26.05\ [min]$$

It should be noted that this time to steady state is simply an estimate; therefore, the technician must pay attention to any major changes to measured values that might suggest steady state has not been achieved.

3.5. Calculating Capture Efficiency

In short, the capture efficiency (CE) is the ratio of the tracer gas removed from the chamber to the tracer gas injected into the chamber and it is calculated by dividing the difference in tracer concentration between the exhaust and the chamber by the difference in concentration between the exhaust and the inlet. This is given by the following equation:

$$CE = \frac{C_E - C_C}{C_E - C_I}$$

For the example data given above, this is calculated as:

$$CE = \frac{5427.9\ [ppm] - 713.2[ppm]}{5427.9\ [ppm] - 441.1\ [ppm]}$$

$$CE = \frac{4714.7\ [ppm]}{4986.8\ [ppm]}$$

$$CE = 0.9454 = 94.54\%$$

3.6. Statistical Calculations within a Test

All the calculations shown above were performed for a single data point taken during a capture efficiency test. Each manual test is composed of 10 of these points and each automated test is composed of approximately 1100 of these points. The reported capture efficiency of a test is the average of the capture efficiency calculated at each test

point, with the average accompanied by a standard deviation, coefficient of variance, and uncertainty. Manual tests containing 10 points each are used for the example calculations below, but the relevant formulae are scaled up as needed for the automated tests. Example calculations are performed for the CE test data presented in Table 3.4.

Table 3.4: Example Test Data

Point	C_I **[ppm]**	C_C **[ppm]**	C_E **[ppm]**	**CE [%]**
1	443	1551	5002	75.70
2	444	1474	5058	77.68
3	444	1542	5023	76.02
4	444	1488	4976	76.96
5	444	1496	4951	76.66
6	446	1512	4959	76.38
7	444	1519	4898	75.31
8	445	1545	5111	76.43
9	444	1540	5255	77.22
10	445	1500	5217	77.89

First, the average is calculated for each of the measurement columns of Table 3.4. This is simply the sum of all measured values divided by the number of measurements, n.

$$CE_{AVG} = \frac{\sum_{i=1}^{n} CE_i}{n}$$

$$CE_{AVG} = \frac{75.70 + 77.68 + \cdots + 77.2 + 77.89}{10}$$

$$CE_{AVG} = 76.62\ \%$$

The sample standard deviation is a measure of how much the data set varies from the mean value calculated above. It is calculated as follows:

$$CE_{SDEV} = \sqrt{\frac{\sum_{i=1}^{n}(CE_i - CE_{AVG})^2}{n-1}}$$

$$CE_{SDEV} = \sqrt{\frac{(75.70 - 76.62)^2 + (77.68 - 76.62)^2 + \cdots + (76.02 - 76.62)^2}{10-1}}$$

$$CE_{SDEV} = 0.83$$

The coefficient of variance is the ratio of the standard deviation to the average and is expressed as a percentage. It is a more relative expression of the data set's deviation from its mean value.

$$CE_{COV} = \frac{CE_{SDEV}}{CE_{AVG}}$$

$$CE_{COV} = \frac{0.83}{76.62}$$

$$CE_{COV} = 0.011 = 1.1\%$$

At the end of a test, the average, standard deviation, and coefficient of variance is calculated for each of the three tracer gas concentration measurements as well as the ten instantaneously calculated capture efficiencies. Table 3.5 organizes these calculated

values for the example case in question. Per the ASTM standard, the reported capture efficiency is calculated using the three averaged tracer gas concentration measurements.

Table 3.5: Example Average, Standard Deviation, and Coefficient of Variance Results

	C_I	C_C	C_E	**CE**
AVG	444	1517	5035	76.62
SDEV	0.82	26.96	133.98	0.83
COV	0.2%	1.8%	2.7%	1.1%

Finally, the uncertainty for the capture efficiency measurement can be calculated using the standard error of the mean (SEM) of the three tracer concentration measurements along with the precision uncertainty of each measurement device. The SEM is found by dividing the standard deviation by the square root of the number of data points. Again, example calculations will be performed for a single parameter, but all results will be summarized in Table 3.6.

$$\delta_{C_I\,SE} = \frac{C_{I-SDEV}}{\sqrt{n}}$$

$$\delta_{C_I\,SE} = \frac{0.82}{\sqrt{10}}$$

$$\delta_{C_I\,SE} = 0.2603$$

The uncertainty of each concentration measurement is taken as the square root of the SEM squared and the precision uncertainty squared. The precision uncertainty of the

inlet and exhaust measurements are taken to be zero per the ASTM standard while the precision uncertainty of the chamber concentration is taken as 1.25% of the mean chamber concentration.

$$\delta_{C_I} = \sqrt{{\delta_{C_I\,SE}}^2 + {\delta_{C_I\,P}}^2}$$

$$\delta_{C_I} = \sqrt{0.2603^2 + 0^2}$$

$$\delta_{C_I} = 0.2603$$

Table 3.6: Tracer Gas Concentration Uncertainties

	C_I	C_C	C_E
δ_{SE}	0.260342	8.525843	42.3665
δ_P	0	18.95875	0
δ	0.260342	20.7876	42.36665

With all this information, the overall capture efficiency uncertainty can be calculated as follows:

$$\delta_{CE} = \frac{CE_{AVG}}{100} * \sqrt{\frac{(\delta_{C_E})^2 + (\delta_{C_C})^2}{(C_{E\_AVG} - C_{C\_AVG})^2} + \frac{(\delta_{C_E})^2 + (\delta_{C_I})^2}{(C_{E\_AVG} - C_{I\_AVG})^2}}$$

$$\delta_{CE} = \frac{76.62}{100} * \sqrt{\frac{(42.36665)^2 + (20.7876)^2}{(5035 - 1517)^2} + \frac{(42.36665)^2 + (0.260342)^2}{(5035 - 444)^2}}$$

$$\delta_{CE} = 0.012478122 = 1.248\%$$

3.7. Statistical Calculations for Comparisons between Test Series

Several t-test using the independent samples method were used to determine whether results between any two of the three test methods (single sensor, three sensor manual, and three-sensor automatic) were statistically similar. In this form of t-test, the t value is calculated as follows:

$$t = \frac{\mu_A - \mu_B}{\sqrt{\left[\frac{\left(\sum_{i=1}^{n} A^2 - \frac{(\sum_{i=1}^{n} A)^2}{n_A}\right) + \left(\sum_{i=1}^{n} B^2 - \frac{(\sum_{i=1}^{n} B)^2}{n_B}\right)}{n_A + n_B - 2}\right] * \left[\frac{1}{n_A} + \frac{1}{n_B}\right]}}$$

As an example, consider the dataset described in Table 3.7:

Table 3.7: Example Data for T-Test

	A	B
1	93.86	93.95
2	93.65	93.99
3	93.17	93.10

The first step in a t-test is to state the null hypothesis, as well as the alternative hypothesis (5). For this example, the null hypothesis is that data sets A and B describe the same mean. The alternate hypothesis is that they describe different means. In the above t-value calculation, μ_A and μ_B are the means of groups A and B, respectively. The

first step in the calculation is to take the sum of each group, the sum of the squares of each element of each data group, and the mean of each data group. This information for this example is assembled in Table 3.8.

Table 3.8: T-Value Calculation Inputs

Symbol	Description	Value
μ_A	Mean of group A	93.56
μ_B	Mean of group B	93.68
$\sum_{i=1}^{n} A^2$	Sum of squares of the elements of group A	26260.671
$\sum_{i=1}^{n} A$	Sum of the elements of group A	280.68
$\sum_{i=1}^{n} B^2$	Sum of squares of the elements of group B	26328.333
$\sum_{i=1}^{n} B$	Sum of the elements of group B	281.04
n_A	Elements in group A	3
n_B	Elements in group B	3

With these preliminary calculations performed, the t value for a test, assuming equal variance, can be calculated as follows:

$$t = \frac{93.56 - 93.68}{\sqrt{\left[\frac{\left(26260.671 - \frac{(280.68)^2}{3}\right) + \left(26328.333 - \frac{(281.04)^2}{3}\right)}{3 + 3 - 2}\right] * \left[\frac{1}{3} + \frac{1}{3}\right]}}$$

$$t = -0.33815$$

Note that the sign of the t value is irrelevant as only its absolute value will be compared. The negative sign simply comes from the arbitrary order in which the data sets were presented.

Next, an alpha level must be selected. This alpha level represents confidence that a type I error has not been made (5). A type I error occurs when a t-test suggests rejecting the null hypothesis, and accepting the alternate hypothesis, in cases where it is incorrect to do so (5). This example will assume an alpha of 0.05 which corresponds to a 95% confidence in the results of the t-test.

The last piece of information needed for the test is the number of degrees of freedom (DOF). For a test assuming equal variance and independent samples, this is simply the number of elements in groups A and B minus two (6). In this case, there are six total elements, so the DOF is four. With this information the tabulated cutoff t-value can be determined for the given alpha and degrees of freedom. In this example the cutoff t-value is 2.776. This tabulated value is greater than the calculated t value, suggesting that the null hypothesis should not be rejected. Therefore, the conclusion of the test is that the two data sets describe the same mean value and are statistically similar.

CHAPTER 4.

DEVELOPMENT OF TESTING METHOD WITH THREE SENSORS

4.1. Test Methods

Two alternate testing methods were developed to evaluate the use of a three-sensor testing system. Both methods use a multi-sensor array to perform those measurements specified in ASTM-E3087 while requiring minimal changes to the established protocol used by REEL. This section will begin by detailing the single-sensor test method as it is outlined in ASTM-E3087 and currently used by the REEL capture efficiency testing facility. Then the two proposed methods evaluated in this study will each be explained and compared to the existing method on which they are based.

4.1.1. Single-Sensor Testing Procedure

The capture efficiency testing procedure and report format are specified in Sections 8 and 9, respectively, of ASTM-E3087. Testing must be performed in a chamber with minimum floor-dimensions of 2.5 meters by 3.5 meters and a height between 2.4 meters and 2.5 meters (2). The chamber should be constructed such that, with its inlets and outlets sealed, it leaks at a rate less than 2.5 air changes per hour under a pressure of 50 Pascals (2).

The chamber must have at least one inlet for ambient air and at least one outlet for range hood exhaust. The inlet should be sized and oriented such that the inlet air has

an average velocity less than 5 meters per second, that incoming air impinges on neither the range hood being tested nor the simulated cooking range, and that chamber depressurization at maximum range hood operating speed does not exceed 5 Pascals (2).

A simulated kitchen counter with electric burners to simulate a kitchen range must be centered on one of the two longer walls of the chamber. These simulated elements should be sized such that their top plane is 0.9 meters above the floor of the chamber, that the counter extends at least 0.5 meters to either side of the range hood of interest, and that the simulated counter and cooking range extend at least 0.65 meters from the chamber wall on which they are mounted (2). The number of electric burners needed as well as the relative spacing between them is determined by the width of the range hood of interest. The heating burners are intended to emulate actual cooking conditions by replicating the buoyant effects of the heated plume of released contaminants (7). In an actual cooking event, contaminants are released by food being heated. Therefore, the plume of tracer gas released in testing must also be heated to accurately simulate cooking conditions.

Each burner must be fitted with an emitter assembly as described in Section 6.2.2 of ASTM-E3087. Figure 4.1 shows the tracer gas emitter assembly as it is depicted in ASTM-E3087. Each emitter is composed of three plates of 254 mm in diameter as well as several metal standoffs. As seen in Figure 4.1, the uppermost and middle plates are fitted together and held above the bottom plate by the metal standoffs. The bottom plate is purely a thermal mass, and it is a solid disc of metal, 12.7 mm thick. The topmost plate is 3 mm thick and must contain at least 30 evenly spaced dispersion holes 3.5 mm

in diameter. In addition, the top plate must have a hole for the injection of tracer gas into the emission assembly. The middle plate must have at least 15 dispersion holes; when fitted to the top plate, there should be a 9.5 mm deep diffusion cavity to allow tracer gas to be emitted equally from the top and bottom of the assembly. The emitters should be centered atop their respective burners and the burners should be placed such that the center of their respective emitters is 500 mm from the back wall of the chamber (2).

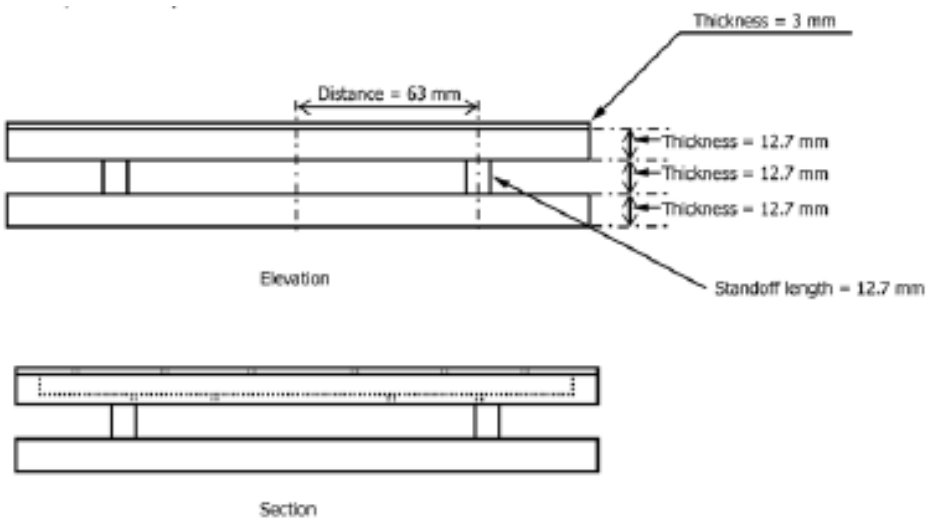

Figure 4.1: Profile view of the tracer gas emitter assembly. Reprinted from Figure 4 of ASTM-E3087 (2)

The range hood of interest is to be appropriately mounted to the wall of the test chamber at a specified height above the burners and tracer gas emitters (2). The testing standard does not specify one universal mounting height for range hoods being tested, so the height of installation is often specified by the range hood manufacturer. The specified height is meant to simulate the fan's position as it would be installed in an

actual kitchen. In general, lower mounting heights increase the average measured CE value but also lead to greater uncertainty (8). Simulated cabinetry coming down from the ceiling must be brought flush against either side of the range hood to approximate actual installation conditions. The hood is then set to the required speed with flow rate being finely adjusted by using dampers and inline fans connected to the exhaust ducting. The power supplied to the burner assemblies is adjusted until an emitter surface temperature of 160±10ºC is maintained under steady state. While the original 2017 release of ASTM-E3087 specifies a temperature of 200±10ºC, this was revised in the release of ASTM-E3087-18 the following year. A subsequent study indicates that while this temperature does not appreciably impact the variability or uncertainty of the test, it can impact the actual measured CE value (9). Once the emitter plates reach the specified surface temperature of 160±10ºC and the test chamber entrance has been sealed, the technician can begin injecting tracer gas. The tracer gas is injected at a rate such that the difference between the exhaust and inlet concentrations at steady state is greater than 1% of the accuracy of the concentration sensor (2). Section 6.2.5 of ASTM-E3087 specifies the maximum allowable injection rate as 0.5% of the airflow rate through the test hood (2). The technician must then wait until steady state has been achieved, defined by four air changes within the chamber. The standard then specifies that the tracer concentrations at the inlet, chamber, and exhaust locations must be measured at least ten times over at least ten minutes (2). The ten measurements for each location are then averaged, along with the flowrate of the range hood, surface temperatures of the emitter plates, and air temperature within the chamber. Upon completion of the test, the

reported capture efficiency is calculated from the averaged CO2 concentration using Equation 1 (2).

The standard does not specify a sampling frequency, but the time required to enter the necessary inputs and switch between measurement locations results in a typical rate of one data point every one to two minutes for REEL technicians. Since each test requires at least ten data points, each capture efficiency test at REEL lasts approximately twenty minutes on average. Technicians typically begin each point by measuring the chamber concentration before switching to measure the exhaust concentration. Once the exhaust concentration is measured the sensor is switched to the inlet sample point. While the inlet measurement stabilizes, the technician can record the flow rate, emitter plate and chamber temperatures, and chamber depressurization. The technician then completes the data point by recording the concentration of tracer gas at the inlet.

While an average test lasts approximately 20 minutes, it is possible for a test to go on far longer if after ten points the technician is not confident in the stability of the measurements. Test stability is typically assessed by plotting the capture efficiency calculated at each point against the point's numbers in the sequence and calculating the slope of the plot's linear trend line. The slope has units of percent-CE per change in test point, and while it roughly describes the gross upward or downward trends in capture efficiency over time during a test it is not a rigorously defined parameter with any direct meaning. If this slope is greater than 0.15 or less than -0.15 the test continues until the most recent ten points satisfy these conditions. Figure 4.2 shows an example of one of these plots with its associated linear trend line, the slope of which indicates a stable test

has been achieved. While this calculated slope does not have a direct meaning, it is a useful tool for gauging whether any major shifts in capture efficiency occurred over the course of testing. The ten most recent points are then averaged and reported.

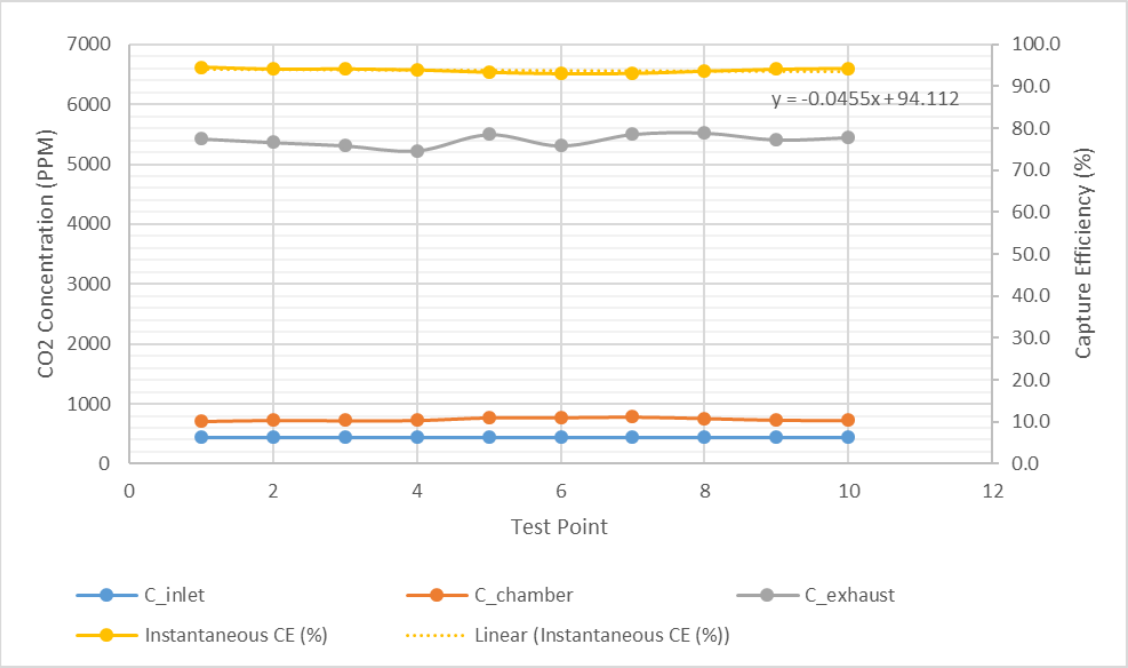

Figure 4.3: An example of the plotted results of a completed capture efficiency test performed at REEL.

4.1.2. Three-Sensor Manual Input Testing

The first proposed variation in the test method as a replacement for the single sensor specified by the standard is the manual collection of data using three concentration sensors. This method was designed to emulate the conventional single-sensor test method as closely as possible with the major difference being the simultaneous display of all measurements because of the use of the three sensors. This method still requires the technician to manually record all measurements needed for each

point of the test. While the need for manual data entry still limits the number of points that can be taken in each test, the elimination of toggling to access all three locations allows the technician to gather each point's component measurements much faster. This approach decreases the difference in the times at which a point's component measurements are made, while also allowing the technician to delay a particular measurement, as in the single-sensor test method, if it is deemed unstable.

In this test method, the technician records one full set of measurements every two minutes, corresponding to one of the ten numbered rows of the table in Figure 4.4. The time required to record a data point is substantially reduced when compared to the single-sensor method, but the approximate time between collected points was maintained to keep methods as similar as possible. Just like the single-sensor test, the ten most recent points have their data averaged and reported. Finally, the capture efficiency calculated from these averages is reported.

No.	C_inlet (ppm)	C_chamber (ppm)	C_exhaust (ppm)	CE	Q_hood (cfm)	Right Burner Temp. (°C)	Left Burner Temp. (°C)	Chamber Temp. (°F)	Depressurization (i.w.c)
Taken after 4 Air Changes				#DIV/0!					
				#DIV/0!					
				#DIV/0!					
				#DIV/0!					
				#DIV/0!					
1	441	536	5445	98.10	301	170	168	76	0.018
2	438	535	5408	98.05	302	170	168	76	0.0176
3	440	527	5392	98.24	302	170	168	76	0.0172
4	440	529	5372	98.20	301	169	168	76	0.0179
5	441	521	5382	98.38	302	168	167	76	0.0176
6	440	515	5485	98.51	303	167	166	76	0.0172
7	441	506	5451	98.70	303	166	165	76	0.0169
8	440	506	5448	98.68	302	166	164	76	0.0178
9	441	510	5441	98.62	303	165	163	76	0.0173
10	440	508	5472	98.65	302	164	162	76	0.0175
Post				#DIV/0!					
Post				#DIV/0!					
Post				#DIV/0!					
Post				#DIV/0!					

Figure 4.4: Example of a manual data entry table

4.1.3. Three-Sensor Automated Testing

The second proposed variation in the test method is an almost entirely automated test. In this method the technician simply waits until the steady state time has been achieved, re-zeros the instruments, and then allows the virtual instrument to record one set of measurements each second to an excel file. After approximately twenty minutes, the technician stops the recording and copies all data from the output file to the test report where it is analyzed. The virtual instrument calculates and records an instantaneous capture efficiency for each point, and the reported capture efficiency is the average of these instantaneous values.

As shown in Figure 4.5, the inlet, chamber, and exhaust concentrations of tracer gas as well as the capture efficiency, burner temperatures, depressurization, and Venturi pressure are all averaged for the duration of the test. Note that for this method the average flow rate is calculated after the test using the average Venturi pressure. In both the single-sensor and multi-sensor manual methods, the volumetric flow rate itself is recorded at each point, instead of the Venturi pressure, and these ten flow rate measurements are averaged at the end of testing. The total number of points collected, as well as the test duration, are displayed in the upper left corner of the report.

1										
2	Elapsed Time (minutes):	19.30								
3	Number of Points	1158								
4		**Inlet (ppm)**	**Chamber (ppm)**	**Exhaust (ppm)**	**CE**	**Right Burner (°C)**	**Left Burner (°C)**	**Depressurization (iwc)**	**Venturi (i.w.c)**	**Q* (cfm)**
5	**Average:**	452.1	2657.6	4931.9	**50.65**	153	168	0.0075	0.186	164
6	STDEV:	0.75	53.18	212.87	2.47	0.47	0.25	0.00	0.00	
7	COV:	0.16%	2.00%	4.32%	4.87%	0.31%	0.15%	6.62%	2.34%	
8		Standard Error Calculation								
9		Inlet		Chamber		Exhaust				
10		**Mean**	452.1135682	**Mean**	2657.57	**Mean**	4931.9			
11		**Sum Dev²**	643.3389201	**Sum Dev²**	3272736	**Sum Dev²**	5E+07			
12		**Std. Dev**	0.745681268	**Std. Dev**	53.185	**Std. Dev**	212.87			
13		**Std. Error**	0.021912854	**Std. Error**	1.56291	**Std. Error**	6.2555			
14		**δ_{se}**	0.021912854	**δ_{se}**	1.56291	**δ_{se}**	6.2555			
15		**δ_p**	0	**δ_p**	33.2197	**δ_p**	0			
16		**δ**	0.021912854	**δ**	33.2564	**δ**	6.2555			
17		Capture Efficiency Uncertainty				0.007569885				
18		Capture Efficiency Uncertainty [%]				0.757				

Figure 4.5: An example of the automatic test report page including average report data, test duration, and the calculated uncertainty of the capture efficiency.

This method is set apart from the other two by the number of points collected. While a manual test will on average be composed of ten points, an automatic test can be

made up of over one thousand individual points. The addition of so many more measurements help to reduce measurement uncertainty and depicts fluctuations in chamber conditions over time with much greater resolution than a comparable test composed of only ten points. Another major difference in this method is that it requires almost no input from the technician after setup is complete. Even though the technician must be present to ensure that no issues occur, they can perform other tasks simultaneously, such as analyzing data from previous tests or preparing additional range hood samples for future testing. In this method, the technician is unable to directly account for random fluctuations in point stability by simply waiting for a more stable measurement. The resulting increase in potential for random outlier measurements in this test method is compensated by the sheer number of points recorded in each test.

The goal of this automatic method is to collect such a high volume of data that the effects of any instantaneous random fluctuations or outliers are minimized. By contrast, the manual multi-sensor method accounts for these potential sources of uncertainty by relying on the technician's ability to record a more stable and consistent, albeit smaller, group of measurements. Again, however, it should be noted that even with the apparent advantages of multi-sensor data collection methods, including the ability to gather data automatically at high speed, neither of the multi-sensor methods are allowable approaches per ASTM-E3087.

Table 4.1: Comparison of multi-sensor approaches to the standard single-sensor method currently used.

Characteristic	Test Approach		
	Standard Single-Sensor	**Multi-Sensor Manual**	**Multi-Sensor Automatic**
Test Duration	~20 minutes	~20 minutes	~20 minutes
Number of points collected for averaging	10	10	>1000
Number of CO2 concentration sensors used	1	3	3
Validity per ASTM-E3087	Valid	Invalid	Invalid
Technician duties during test	• Toggle gas sampling position • Maintain steady emitter temperatures. • Record measurements • Ensure no issues arise during the test	• Maintain steady emitter temperatures. • Record measurements • Ensure no issues arise during the test	• Maintain steady emitter temperatures. • Ensure no issues arise during the test

CHAPTER 5.

COMPARING RESULTS OF MULTI-SENSOR TEST METHODS TO SINGLE-SENSOR REFERENCE DATA

This section describes the validation testing of the two different multi-sensor methods proposed above. First, the sample range hoods used in testing are listed and assigned an identification number. Then the results are summarized and broken up by test method. Finally, the results are compared to determine statistical similarity between test methods and assess the repeatability of each.

5.1. Samples Used in Testing

The two sample range hoods selected for comparison testing against archive single-sensor data are listed in Table 5.1. The selected samples display several common discharge configurations, design geometries, and mounting heights seen in commercially available residential range hoods. Each of these test samples have an overall nominal width of 30 inches, which was kept the same to avoid the rearrangement of burners and emitters required when wider or narrower hoods are tested.

Table 5.1: Range Hoods Used in Multi-Sensor Method Validation Testing

	Manufacturer & Model	Discharge	Mounting Height (in.)	Notes
1	Venmar Ispira: IU600ES30BL	Vertical Rectangular (3.25”x10”)	24	Under-cabinet range hood; 4 speeds
2	Whirlpool: WMH31017HB	Vertical Rectangular (3.25”x10”)	18	OTR Microwave; 2 speeds

5.2. Overall Data Summary

These two sample units were tested several times at a total of five operating speeds. Table 5.2 summarizes all test results obtained for the manual three-sensor testing method, while Table 5.3 summarizes the same data for the tests performed using the three-sensor automatic test method. Both Table 5.2 and Table 5.3 also show statistical data such as the average and standard deviation of results for each test series. The three sensor methods were able to be tested simultaneously by recording the automatic test in the background during each manual tests. This greatly reduced the amount of time required to complete each test series. Finally, single sensor reference data was gathered for the samples from several previously completed tests, with a summary of these results being shown in Table 5.4.

Table 5.2: Manual Multi-Sensor Results for Comparison to Single-Sensor Reference Data

Sample	Flow Rate (cfm)	Test 1 CE (%)	Test 2 CE (%)	Test 3 CE (%)	Average CE (%)	SDEV
1	350	93.9	93.7	93.2	93.6	0.354
1	300	80.0	79.1	81.8	80.3	1.33
1	160	51.3	51.5	--	51.4	0.163
2	250	63.9	63.7	65.1	64.2	0.771
2	201	52.9	56.2	55.9	55.0	1.82

Table 5.3: Automatic Multi-Sensor Results for Comparison to Single-Sensor Reference Data

Sample	Flow Rate (cfm)	Test 1 CE (%)	Test 2 CE (%)	Test 3 CE (%)	Average CE (%)	SDEV
1	350	94.0	94.0	93.1	93.7	0.503
1	300	79.8	79.3	81.2	80.1	0.944
1	160	51.1	51.4	--	51.2	0.156
2	250	63.5	64.5	66.5	64.8	1.51
2	201	52.4	56.1	56.1	54.9	2.15

Table 5.4: Single-Sensor Reference Data for Comparison to Multi-Sensor Results

Sample	Flow Rate (cfm)	Test 1 CE (%)	Test 2 CE (%)	Test 3 CE (%)	Average CE (%)	SDEV
1	350	92.66	94.17	94.50	93.78	0.981
1	300	82.92	80.79	82.77	82.16	1.189
1	160	50.12	46.33	46.34	47.60	2.185
2	250	64.52	--	--	64.52	--
2	201	54.15	56.55	58.31	56.34	2.088

Figure 5.1 compares the average capture efficiency reported by each test method in test configurations for which single-sensor reference data could be acquired. As this plot shows, all three methods yielded similar results in all cases tested.

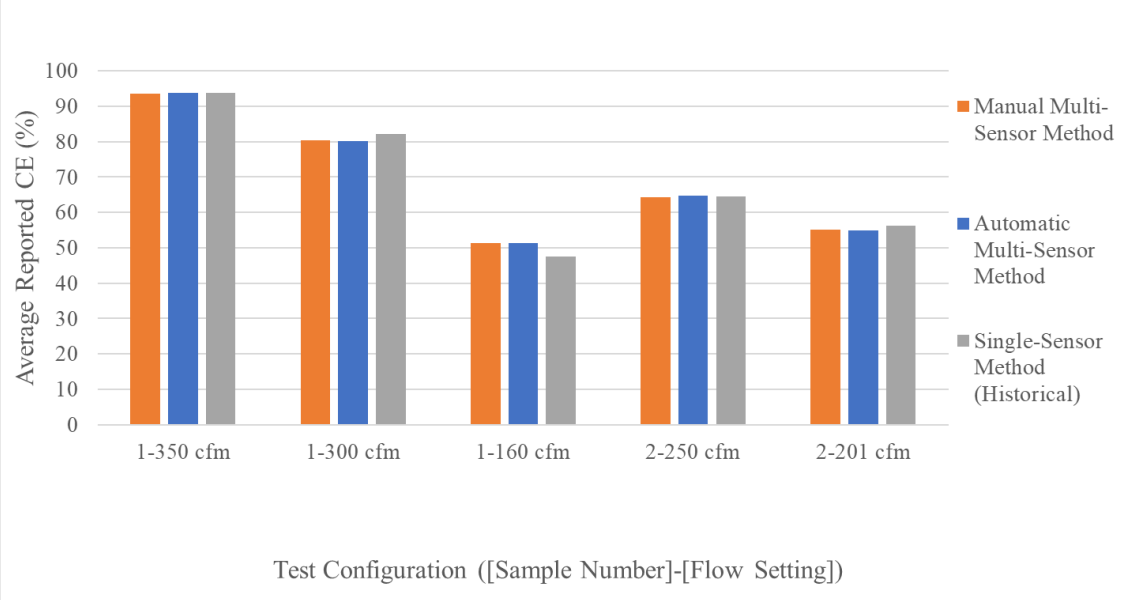

Figure 5.1: Comparison of average capture efficiency reported by each multi-sensor method to single-sensor reference data.

The absolute and percentage difference in reported results were then calculated between the single-sensor method and the multi-sensor methods for each of the

corresponding test cases. These comparisons between the single-sensor and the multi-sensor manual methods are assembled in Table 5.5, and the corresponding comparisons between the single-sensor and multi-sensor automatic methods are assembled in Table 5.6. The absolute differences between the single-sensor and each of the multi-sensor methods were then plotted as Figure 5.2 and the respective percentage differences plotted as Figure 5.3.

Table 5.5: Comparison of Average Capture Efficiency Reported between Single-Sensor and the Manual Multi-Sensor Method

Sample	Flow Rate (cfm)	Single-Sensor AVG CE (%)	Manual Multi-Sensor AVG CE (%)	ΔCE_AVG (%)	CE_AVG (%)	%DIF
1	350	93.8	93.6	0.220	93.7	0.235
1	300	82.2	80.3	1.85	81.2	2.28
1	160	47.6	51.4	3.80	49.5	7.68
2	250	64.5	64.2	0.320	64.4	0.497
2	201	56.3	55.0	1.32	55.7	2.37

Table 5.6: Comparison of Average Capture Efficiency Reported between Single-Sensor and the Automatic Multi-Sensor Method

Sample	Flow Rate (cfm)	Single-Sensor AVG CE (%)	Auto Multi-Sensor AVG CE (%)	ΔCE_AVG (%)	CE_AVG (%)	%DIF
1	350	93.8	93.7	0.100	93.7	0.107
1	300	82.2	80.1	2.07	81.1	2.55
1	160	47.6	51.2	3.64	49.4	7.37
2	250	64.5	64.8	0.280	64.7	0.433
2	201	56.3	54.9	1.49	55.6	2.68

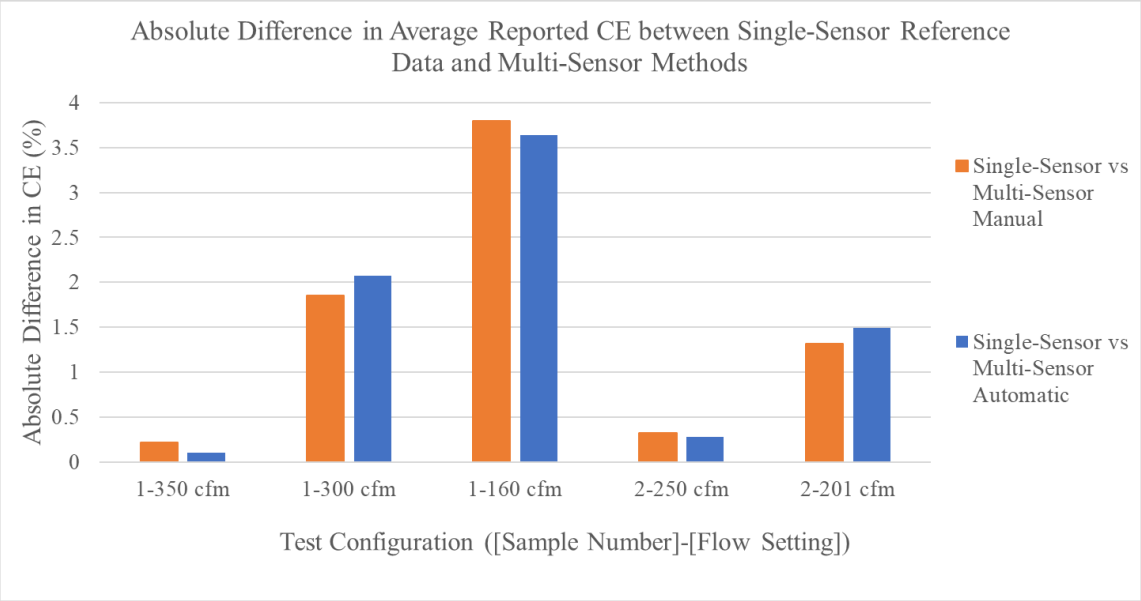

Figure 5.2: Comparison of absolute difference in average reported capture efficiency between the single-sensor method and each of the multi-sensor methods

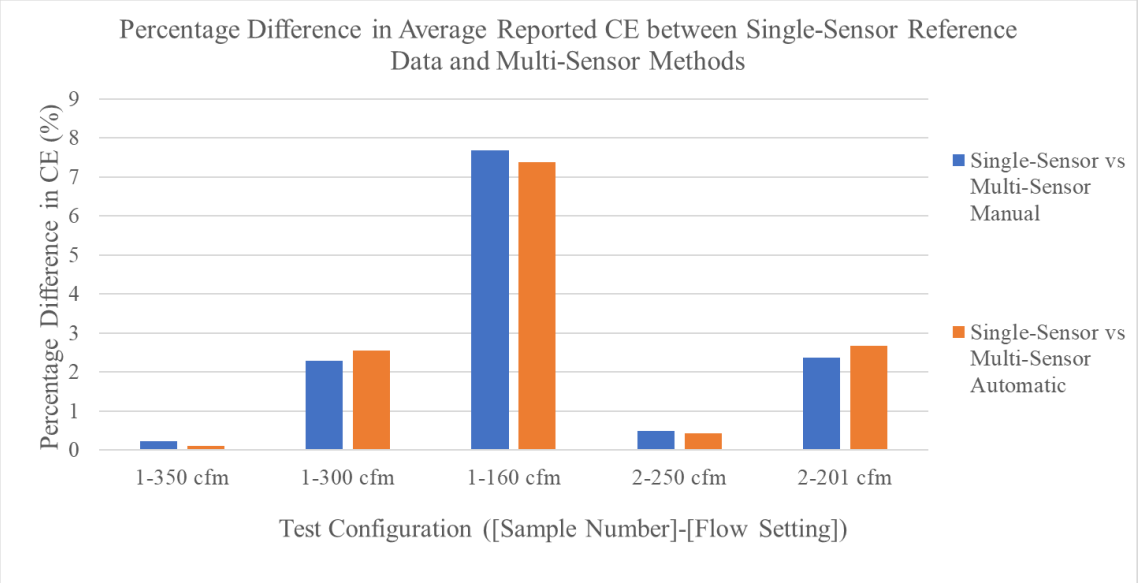

Figure 5.3: Comparison of the percentage difference in average reported capture efficiency between the single-sensor method and each of the multi-sensor methods

As shown in Table 5.4, the standard deviation for each respective testing configuration was calculated for the historical single-sensor test data. Just as with the average reported results, the standard deviation of the respective test series in comparable testing configurations was plotted in Figure 5.4 to compare the repeatability of the single-sensor method to those of the two multi-sensor methods. Note that the standard deviation could not be calculated for the results of single-sensor testing on sample range hood 2 at 250 cfm, as there is only one archive test available for comparison in this configuration. In addition, it should be noted that the plot in Figure 5.4 for sample range hood 1 at a speed of 160 cfm shows standard deviation calculated for a series of three tests using the single sensor method but only series of two tests using the multi-sensor methods. As Figure 5.4 shows, the single sensor method produced the highest standard deviation in two cases, while the manual and automatic multi-sensor methods produced the highest standard deviation in one case each.

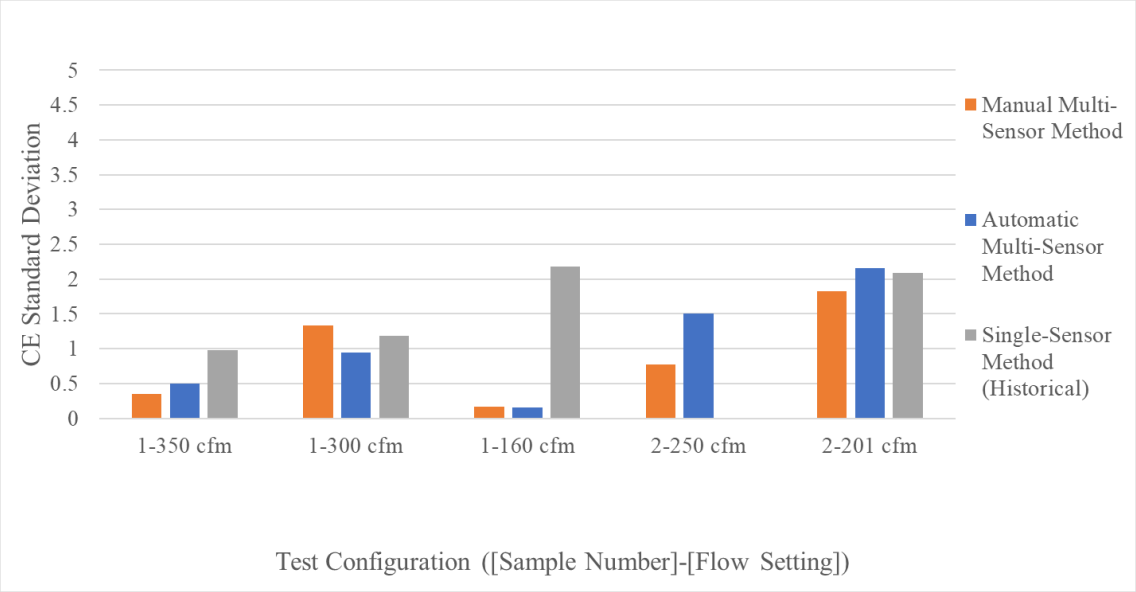

Figure 5.4: Comparison of the standard deviations for each of the three test methods in comparable configurations. (Note the reference test standard deviation for sample 2 at 250 cfm could not be calculated.)

5.3. Hypothesis Testing to Determine Similarity of Results

Two groups of t-tests were performed to assess the statistical similarity of each multi-sensor testing method to the reference single-sensor dataset. The single-sensor method was compared first to the three-sensor manual method and then to the automatic method. Table 5.7 contains the relevant data for comparison between the single-sensor and three-sensor manual test procedures. Only one test was performed at 250 cfm on sample 2, so a meaningful comparison for this configuration was not possible.

Table 5.7: Data Needed for t-test between Single-Sensor and Multi-Sensor Manual Test Methods

		3 Sensor Manual			Single Sensor		
Sample	Flow Rate (cfm)	Average	SDEV	N	Average	SDEV	N
1	350	93.56	0.354	3	93.78	0.981	3
1	300	80.31	1.331	3	82.16	1.189	3
1	160	51.40	0.163	2	47.60	2.185	3
2	201	55.02	0.771	3	56.34	2.088	3

A two-sample t-test assuming unequal variance was then performed for each sample at each tested speed. The null hypothesis of this comparison is that the results produced by the three-sensor test are statistically similar to those produced with the single sensor test. The alternate hypothesis is that they are significantly different. The results of this series of t-tests are summarized in Table 5.8 for a confidence of 95%, or an alpha value of 0.05. For each t-test, the null hypothesis is rejected if either the p-value is less than the specified alpha or if the absolute value of the calculated t-statistic is greater than the critical t value.

Table 5.8: Results of t-test Comparing Single-Sensor and Multi-Sensor Manual Results.

Sample	Flow Rate (cfm)	T-statistic (calculated)	DOF	T_{crit}	P-value	Accept/Reject Null Hypothesis
1	350	-0.360	3	3.182	0.743	Accept
1	300	-1.792	4	2.776	0.148	Accept
1	160	2.998	2	4.303	0.096	Accept
2	201	-0.825	4	2.776	0.456	Accept

As Table 5.8 shows, the null hypothesis can be accepted for all four of the compared cases. This suggests that in all cases tested the single-sensor and multi-sensor manual methods were equivalent and reflected the same mean value.

The single-sensor method was then compared to the multi-sensor automatic method by hypothesis testing. Table 5.9 contains the relevant data for this comparison. As in the comparison between the single-sensor and manual multi-sensor methods, the null hypothesis is that the results produced by the automatic test are statistically similar to those produced in the reference single-sensor test. The alternate hypothesis is that the results are significantly different. This set of results for a 95% confidence is summarized in Table 5.10.

Table 5.9: Data needed for t-test between Single-Sensor and Multi-Sensor Automatic Test Methods

		3-Sensor Automatic			Single Sensor		
Sample	Flow Rate (cfm)	Average	SDEV	N	Average	SDEV	N
1	350	93.68	0.503	3	93.78	0.981	3
1	300	80.09	0.944	3	82.16	1.189	3
1	160	51.24	0.156	2	47.60	2.185	3
2	201	54.85	2.154	3	56.34	2.088	3

Table 5.10: Results from t-test Comparing Single-Sensor and Automatic Multi-Sensor Methods

Sample	Flow Rate (cfm)	T-statistic (calculated)	DOF	T_{crit}	P-value	Accept/Reject Null Hypothesis
1	350	-0.152	3	3.182	0.889	Accept
1	300	-2.362	4	2.776	0.078	Accept
1	160	2.877	2	4.303	0.103	Accept
2	201	-0.860	4	2.776	0.438	Accept

As Table 5.10 shows, the null hypothesis is accepted for all cases tested, suggesting that the results obtained with the automatic multi-sensor method are statistically similar to those obtained with the single-sensor method. As a result, both the manual and the automatic multi-sensor methods can be confirmed as equivalent to the single-sensor method for the assumed 95% confidence level.

CHAPTER 6.

COMPARING RESULTS BETWEEN MULTI-SENSOR METHODS

This section describes a comparison of the two different multi-sensor methods proposed above to determine which, if either, of the two is more repeatable. First, the sample range hoods used in testing are listed and assigned an identification number. Then the results are summarized and broken up by test method. Finally, the results are compared to determine statistical similarity between test methods and assess the repeatability of each.

6.1. Samples Used in Testing

A total of five sample range hoods were selected for testing. The selected samples display several common discharge configurations, design geometries, and mounting heights seen in commercially available residential range hoods. It should be noted that each selected sample has an overall nominal width of 30 inches, which was kept the same to avoid the rearrangement of burners and emitters required when wider or narrower hoods are tested. The selected sample units are listed in Table 6.1 along with their code numbers, mounting and discharge details, and design type.

Table 6.1: Range Hoods Used in Multi-Sensor Comparison Testing

	Manufacturer & Model	Discharge	Mounting Height (in.)	Notes
1	Venmar Ispira: IU600ES30BL	Vertical Rectangular (3.25”x10”)	24	Under-cabinet range hood; 4 speeds
2	Whirlpool: WMH31017HB	Vertical Rectangular (3.25”x10”)	18	OTR Microwave; 2 speeds
3	Panasonic: NN-SE284B	Vertical Rectangular (3.25”x10”)	16	OTR Microwave; 4 speeds

Table 6.1 Continued

	Manufacturer & Model	Discharge	Mounting Height (in.)	Notes
4	GE: UVW8301	Vertical 8” Round	24	Wall-mounted range hood; 3 speeds
5	Broan NuTone: AHDA130SS	Vertical 7” Round	24	Under-cabinet range hood; 3 speeds

6.2. Overall Data Summary

Each of the five sample units were tested several times at different operating speeds. Table 6.2 summarizes all test results obtained for the manual three-sensor testing method, while Table 6.3 summarizes the same data for the tests performed using the three-sensor automatic test method. Both Table 6.2 and Table 6.3 also show statistical data such as the average and standard deviation of results for each configuration.

Table 6.2: Summary of Multi-Sensor Manual Comparison Test Results

Sample	Flow Rate (cfm)	Test 1 CE (%)	Test 2 CE (%)	Test 3 CE (%)	Average CE (%)	SDEV
1	350	93.9	93.7	93.2	93.6	0.354
1	300	80.0	79.1	81.8	80.3	1.33
1	160	51.3	51.5	--	51.4	0.163
2	250	63.9	63.7	65.1	64.2	0.771
2	201	52.9	56.2	55.9	55.0	1.82
3	270	68.7	72.2	--	70.5	2.43
3	170	38.5	40.3	--	39.4	1.26
3	140	30.8	33.9	--	32.4	2.14
4	300	85.9	91.0	94.3	90.4	4.23
4	160	52.2	56.8	50.9	53.3	3.07
5	300	93.6	92.3	92.7	92.9	0.671
5	160	52.3	51.3	51.0	51.5	0.637

Table 6.3: Summary of Multi-Sensor Automatic Comparison Test Results

Sample	Flow Rate (cfm)	Test 1 CE (%)	Test 2 CE (%)	Test 3 CE (%)	Average CE (%)	SDEV
1	350	94.0	94.0	93.1	93.7	0.503
1	300	79.8	79.3	81.2	80.1	0.944
1	160	51.1	51.4	--	51.2	0.156
2	250	63.5	64.5	66.5	64.8	1.51
2	201	52.4	56.1	56.1	54.9	2.15
3	270	69.4	72.0	--	70.7	1.87
3	170	36.9	40.3	--	38.6	2.44
3	140	31.2	35.7	--	33.5	3.19
4	300	86.0	92.2	94.1	90.8	4.27
4	160	52.3	56.5	50.3	53.0	3.15
5	300	93.5	92.4	92.8	92.9	0.569
5	160	51.2	50.7	51.6	51.2	0.470

The average capture efficiencies reported by each of the two methods were then compared for each test case, as shown in Table 6.4. First, the absolute value of the difference between CE measured by each of the two methods was calculated for each condition. Each absolute difference between reported capture efficiencies was then divided by the average of the two results to calculate the percentage difference in CE measurements between the two multi-sensor test methods.

Table 6.4: Comparison of Average Reported CE from Multi-Sensor Test Methods

Sample	Flow Rate (cfm)	Manual AVG CE (%)	Auto AVG CE (%)	ΔCE_AVG (%)	CE_AVG (%)	%DIF
1	350	93.6	93.7	0.12	93.6	0.128
1	300	80.3	80.1	0.22	80.2	0.274
1	160	51.4	51.2	0.16	51.3	0.312
2	250	64.2	64.8	0.62	64.5	0.961
2	201	55.0	54.9	0.17	54.9	0.309
3	270	70.5	70.7	0.25	70.6	0.354
3	170	39.4	38.6	0.82	39.0	2.102
3	140	32.4	33.5	1.12	32.9	3.402
4	300	90.4	90.8	0.38	90.6	0.420

Table 6.4 Continued

Sample	Flow Rate (cfm)	Manual AVG CE (%)	Auto AVG CE (%)	ΔCE_AVG (%)	CE_AVG (%)	%DIF
4	160	53.3	53.0	0.28	53.2	0.527
5	300	92.9	92.9	0.02	92.9	0.022
5	160	51.5	51.2	0.39	51.3	0.760

In Figure 6.1 the average capture efficiency reported by each of the two multi-sensor test methods is plotted for direct comparison. The absolute difference in capture efficiency is plotted in Figure 6.2 and the percentage difference between the methods is plotted in Figure 6.3. While the absolute and percentage differences are represented similarly, the absolute difference refers to the absolute value of the difference between two measured capture efficiencies while the percentage difference represents this absolute difference normalized by the average of the two measurements. As all three of these figures indicate, the multi-sensor test methods achieved similar results, with only two out of the twelve cases compared showing a percentage difference in results greater than one percent. In fact, as shown in Figure 6.3, eight out of the twelve cases had a percentage difference less than 0.4 %.

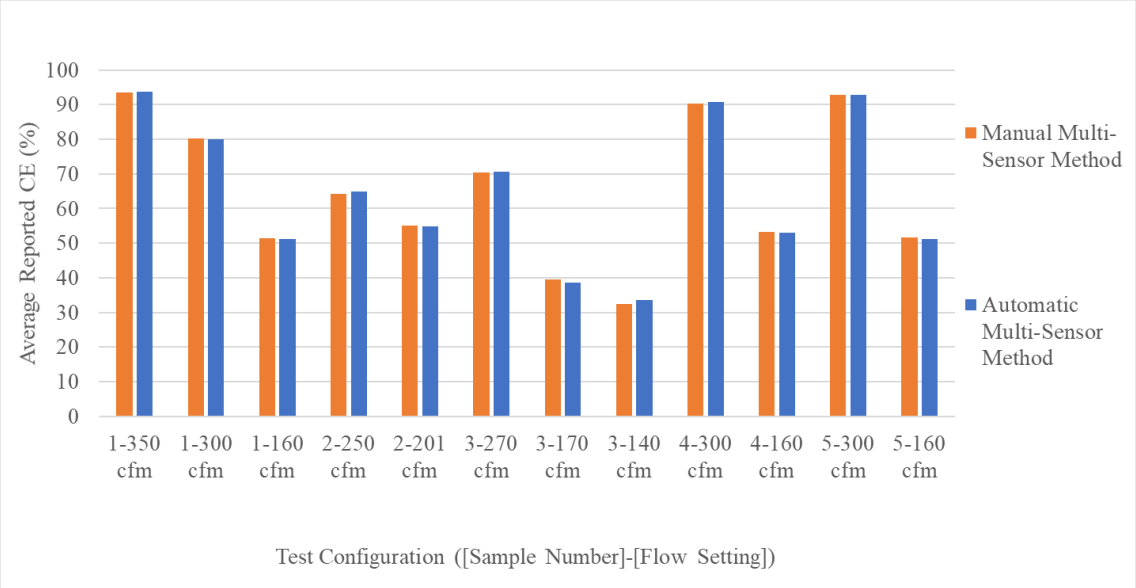

Figure 6.1: Comparison of Average CE Reported by each Multi-Sensor Method

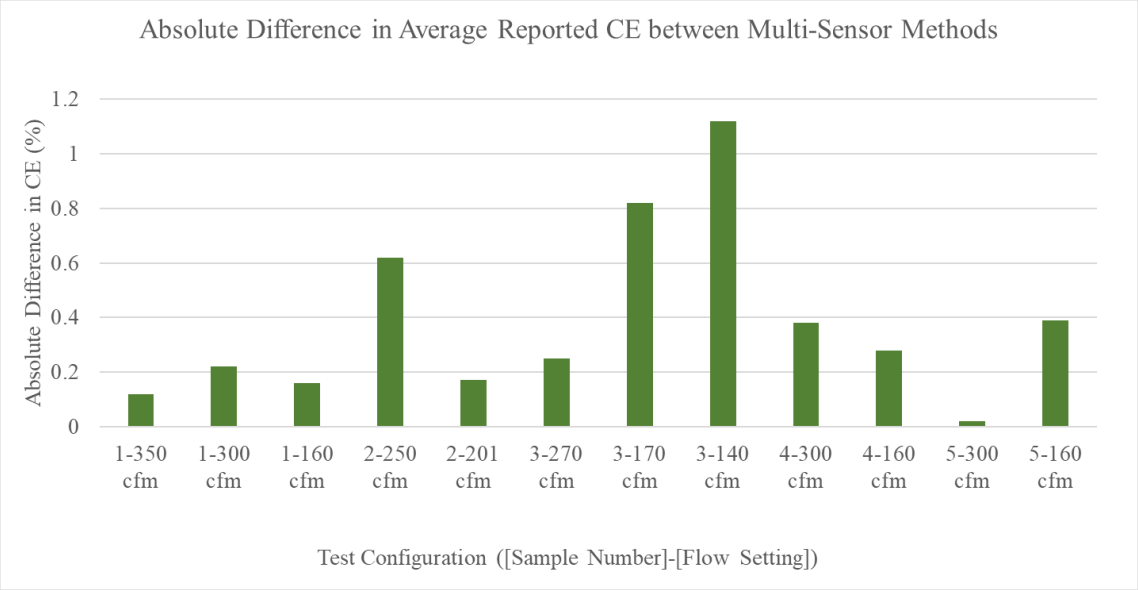

Figure 6.2: Absolute Difference in Average Reported CE between Multi-Sensor Methods

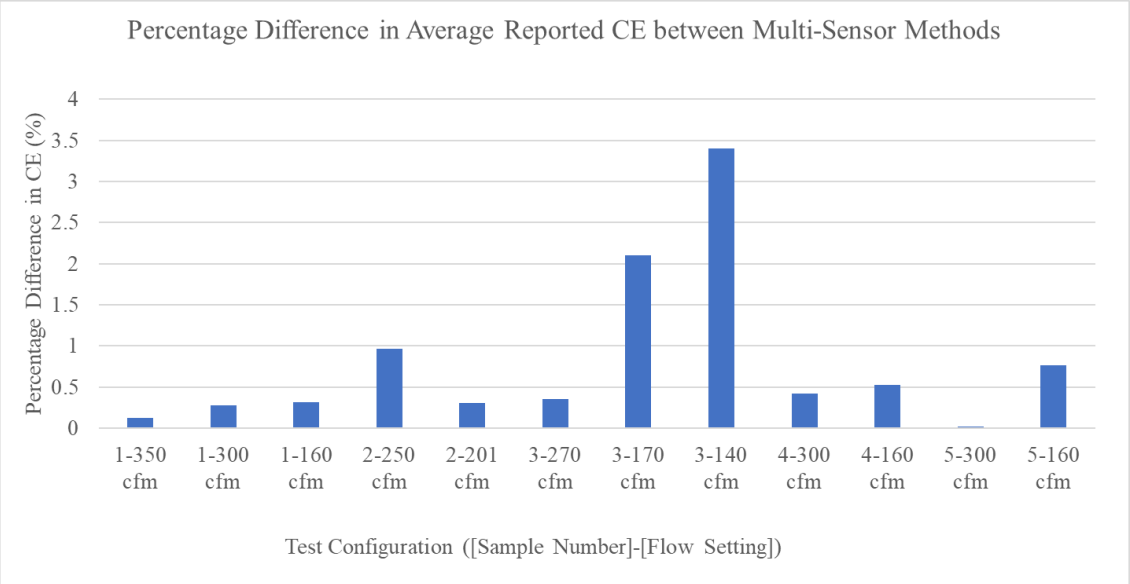

Figure 6.3: Percentage Difference in Average Reported CE between Multi-Sensor Methods

In addition to the average capture efficiency reported by iterative testing performed with each of the multi-sensor methods, the standard deviations of these iterative results were also calculated and plotted in Figure 6.4. This deviation is a representation of the random variation between individual test runs that is seen when using each of the respective testing methods. The automatic method tends to produce slightly more variable measurements of capture efficiency than its manual counterpart. This variability is depicted by the plot in Figure 6.4, wherein the automatic method's standard deviation exceeds that of the manual method in eleven of the twenty cases compared. Moreover, the automatic method yielded results with a standard deviation of 1.77% on average while the manual method produced results with a standard deviation of 1.57% on average.

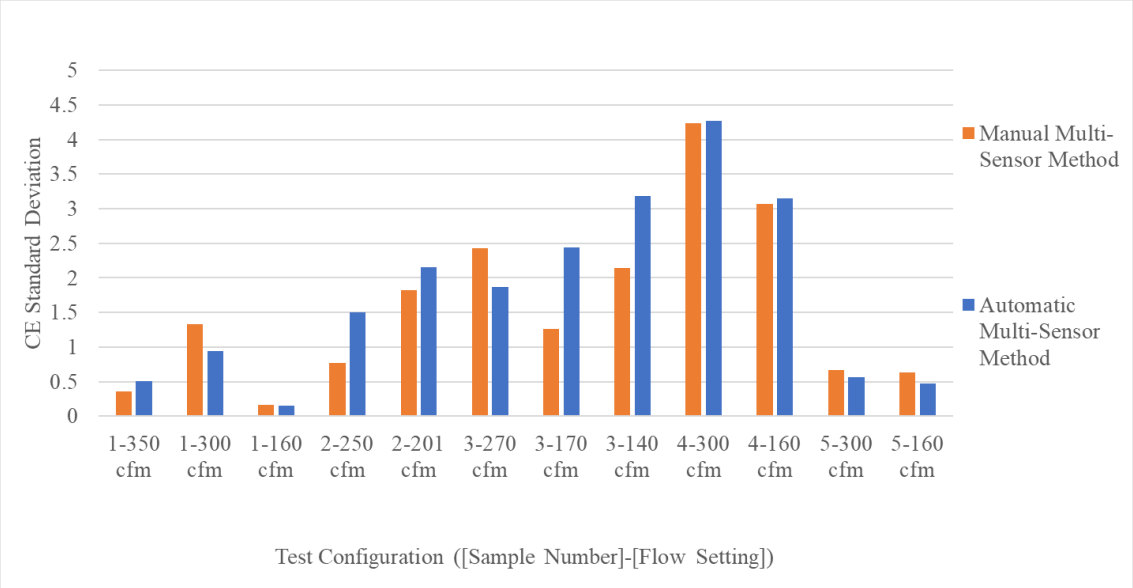

Figure 6.4: Comparison of Standard Deviation of Test Series Performed with Multi-Sensor Methods

6.3. Hypothesis Testing to Determine Similarity of Results

Comparisons between the multi-sensor methods and the single sensor method required a t-test assuming unequal variances because the individual tests being compared were distinct and not always directly comparable. However, all results obtained with the multi-sensor methods can be directly compared to each other. Each iteration of each test was run simultaneously using the manual and automatic three sensor test methods, so the results produced by these two methods can be directly compared to determine equivalence between the two methods. The data needed for this comparison is shown in Table 6.5.

Table 6.5: Data for t-test to Determine Equivalence of Multi-Sensor Methods

		3-Sensor Manual			3-Sensor Automatic		
Sample	Flow Rate (cfm)	Average	SDEV	N	Average	SDEV	N
1	350	93.56	0.354	3	93.68	0.503	3
1	300	80.31	1.331	3	80.09	0.944	3
1	160	51.40	0.163	2	51.24	0.156	2
2	250	64.20	0.771	3	64.82	1.507	3
2	201	55.02	1.822	3	54.85	2.154	3
3	270	70.45	2.425	2	70.70	1.874	2
3	170	39.42	1.259	2	38.60	2.440	2
3	140	32.36	2.143	2	33.48	3.189	2
4	300	90.37	4.232	3	90.75	4.269	3
4	160	53.32	3.070	3	53.04	3.150	3
5	300	92.87	0.671	3	92.89	0.569	3
5	160	51.54	0.637	3	51.15	0.470	3

A series of two sample t-tests assuming equal variance was then performed. The null hypothesis is that the results produced by both methods produce statistically similar results and the alternate hypothesis is that the results are significantly different. This form of t-test is valid in this case because there are an exactly equal number of tests performed using each method and they showed a very similar variance of results. Table 6.6 summarizes the results of this comparison.

Table 6.6: Results of Two-Sample t-tests Showing Equivalence of Multi-Sensor Methods

Sample	Flow Rate (cfm)	T-statistic (calculated)	DOF	T_{crit}	P-value	Accept/Reject Null Hypothesis
1	350	-0.338	4	2.776	0.752	Accept
1	300	0.237	4	2.776	0.825	Accept
1	160	0.974	2	4.303	0.433	Accept
2	250	-0.634	4	2.776	0.560	Accept
2	201	0.107	4	2.776	0.920	Accept
3	270	-0.115	2	2.776	0.919	Accept
3	170	0.425	2	2.776	0.712	Accept

Table 6.6 Continued

Sample	Flow Rate (cfm)	T-statistic (calculated)	DOF	T_{crit}	P-value	Accept/Reject Null Hypothesis
3	140	-0.412	2	2.776	0.720	Accept
4	300	-0.110	4	2.776	0.918	Accept
4	160	0.110	4	2.776	0.918	Accept
5	300	-0.046	4	2.776	0.966	Accept
5	160	0.853	4	2.776	0.442	Accept

These results suggest that the two multi-sensor methods produce results that are statistically similar. This result is in accordance with expectations based on observation and proves that the two proposed multi-sensor sampling methods are equivalent to each other. The future recommendation and selection of the best method for adoption will depend on a thorough analysis of any number of other considerations, with many mentioned and discussed herein, including test times, reliability, repeatability, and various procedural aspects

CHAPTER 7.

USING MULTI-SENSOR METHODS TO CHARACTERIZE IMPACTS OF CHAMBER HARDWARE MODIFICATIONS

After completing the validation testing of the two multi-sensor methods, a separate investigation was launched to determine the sensitivity of capture efficiency results to several seemingly minor changes to the hardware fixtures in the chamber. The goal of this study was to identify the specific cause of deviations between test results acquired before and after a series of modifications to the CE test chamber at REEL. These modifications were done to ensure compliance with ASTM-E3087. The most notable of these modifications are listed in detail in Table 7.1, however, a summary includes the simulated countertop being lowered, and the electric burners being installed inside of it such that the top surface of each emitter assembly was on the same plane as the countertop. These changes were seemingly minor, but several tests performed after the modifications reported markedly lower capture efficiencies when compared to otherwise identical tests performed prior to the modifications.

Table 7.1: Descriptions of Changes Made to the CE Test Chamber Hardware at REEL

	Countertop Height (inches)	Emitter Surface Height (inches)	Emitter Center-to-Back Wall Distance (inches)
Prior to November 2019 Modifications	39.37	45.37	17.69
After Modifications	35.43	35.43	19.69

Testing for this investigation was performed on Sample 4 as described in Table 6.1. This sample is a GE range hood, model UVW8301, with a vertical 8-inch diameter round discharge mounted at a height of 24 inches above the emitter assembly. It should be noted that the changes in Table 7.1 occurred in increments with a number of configuration changes and stops taking place, with tests occurring at each.

7.1. Summary of Test Chamber Configurations

In this study, three phases of changes were made to the testing chamber at REEL in attempt to temporarily recreate its layout prior to the modifications. Each of these phases, representing increments of change, was given a chamber code letter, as summarized in Table 7.2.

Table 7.2: Summary of REEL CE Test Chamber Configurations.

		Countertop Height (inches)	Emitter Surface Height (inches)	Emitter Center-to-Back Wall Distance (inches)	Additional Fixture Sealing Used
Pre-Modification		39.37	45.37	17.69	No
Chamber Code	A	35.43	35.43	19.69	No
	B	35.43	41.43	17.69	No
	C	39.37	45.37	17.69	No
	D	39.37	45.37	17.69	Yes

First, the default condition of the chamber after the modifications was designated chamber code A, which is the configuration used for all testing performed for the multi-sensor validation and comparison studies discussed previously. In this configuration, the

electric burners are embedded in the countertop such that the top surfaces of the emitters are on the same plane as that of the countertop and the center of each emitter is located approximately 19.69 inches, or 500 mm, from the back wall of the chamber.

For chamber code B, each burner was placed on the surface of the countertop and moved approximately two inches closer to the back wall of the chamber. The combined height of each burner and its emitter assembly is 6 inches, so placing the burners atop instead of inside the counter raises the total elevation of the emitter surface by 6 inches. Note that the mounting height of the range hood was adjusted to maintain a spacing of 24 inches between it and the raised emitter assemblies.

The burners and emitters were left atop the counter for chamber code C, but in this configuration, the entire counter was raised by approximately 4 inches. As a result, the total height of the countertop in this configuration is 39.37 inches and the total height of the emitters' top surfaces is 45.37 inches. Again, the range hood sample was raised accordingly to maintain 24 inches of spacing between it and the emitter assemblies.

Chamber code D is virtually identical to chamber code C, with the only difference between the two being that in chamber code D the interfaces between the range hood, simulated cabinetry, and back wall of the chamber are sealed with masking tape to prevent flow around the sides of the range hood.

7.2. Summary of Results

Using the manual multi-sensor test method, described previously, several tests were performed on range hood sample 4 at both of its previously tested speeds in each of

the four specified chamber configurations. In addition, three pre-modification tests performed on this sample at each operating speed were identified for comparison. The results of these tests are detailed in Table 7.3. To briefly summarize, all three experimental chamber configurations, codes B, C, and D, produced results higher than those measured under chamber code A, which as mentioned is the present configuration.

Table 7.3: Summary of Chamber Modification Impact Study Results Acquired using the Manual Multi-Sensor Test Method

Chamber Code	Flow Rate (cfm)	Test 1 CE (%)	Test 2 CE (%)	Test 3 CE (%)	Average CE (%)	SDEV
Pre-Mod	300	91.0	94.2	95.0	93.4	2.12
	160	71.0	72.8	70.1	71.3	1.37
A	300	85.9	91.0	94.3	90.4	4.23
	160	52.2	56.8	50.9	53.3	3.07
B	300	97.2	97.0	97.0	97.0	0.101
	160	71.2	73.1	73.1	72.5	1.09
C	300	97.2	98.4	98.3	98.0	0.695
	160	76.3	71.4	70.6	72.8	3.07
D	300	99.4	99.4	--	99.4	0.035
	160	76.5	73.8	--	75.1	1.88

The average reported capture efficiencies measured at the 300-cfm operating speed for each chamber configuration were then plotted as shown in Figure 7.1 while the average results from the 160-cfm setting are shown in Figure 7.2.

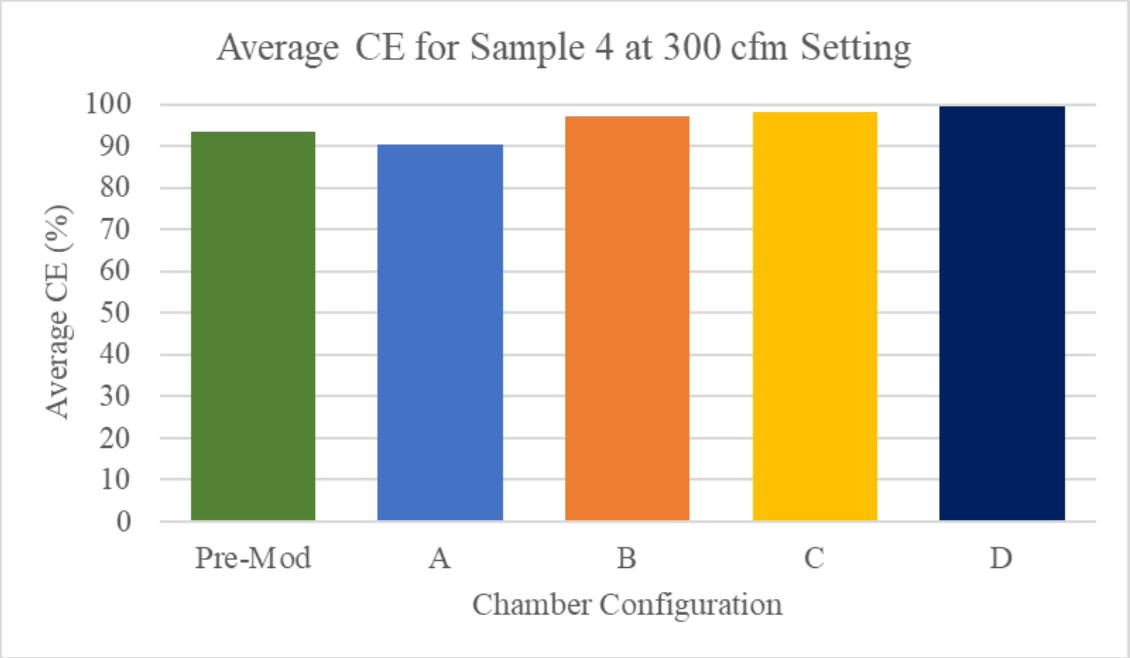

Figure 7.1: Average reported CE for range hood Sample 4 at the 300-cfm setting in each specified chamber configuration.

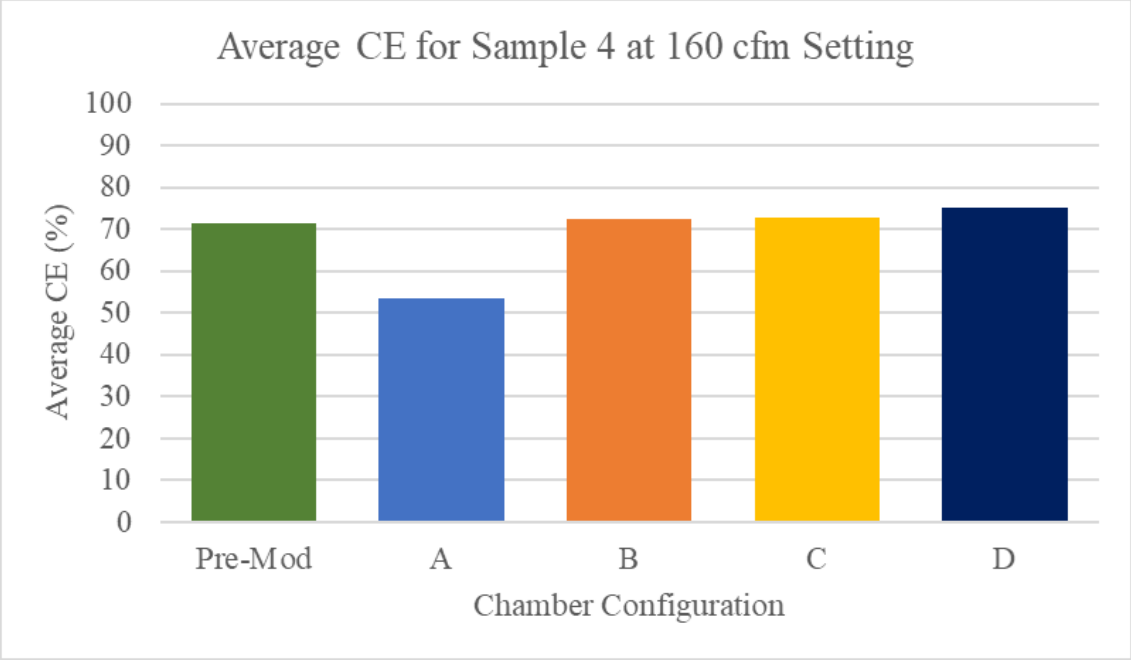

Figure 7.2: Average reported CE for range hood Sample 4 at the 160-cfm setting in each specified chamber configuration.

Next, the average results obtained in each chamber configuration were compared to the historical reference data. The absolute and percentage differences were calculated between data gathered in each respective chamber configuration and the pre-modification historical results. These differences are assembled in Table 7.4. As this table shows, chamber code B appears to produce results that have the closest match to historical reference test data.

Table 7.4: Comparison of absolute and relative difference of experimental chamber hardware configurations from historical reference data

Chamber Code	Flow Rate (cfm)	Absolute Difference from Reference CE (%)	Percentage Difference from Reference CE (%)
A	300	3.0 %	3.3 %
	160	18.0 %	28.9 %
B	300	3.6 %	3.8 %
	160	1.2 %	1.7 %
C	300	4.6 %	4.8 %
	160	1.5 %	2.1 %
D	300	6.0 %	6.2 %
	160	3.8 %	5.2 %

Chamber code A produced results closest to the reference tests at high-speed. However, results at low speed in this configuration were less by approximately eighteen (absolute) percent than was measured historically. Chamber codes C and D produced results higher than the reference test, with the high-speed tests in chamber code D nearly achieving one hundred percent capture efficiency, as seen in Figure 7.2.

The most important result of this study is related to the markedly lower capture efficiency measured at low speed in chamber code A. With the chamber in

configuration A, the sample range hood yielded an average capture efficiency of just over fifty three percent at the 160-cfm operating speed. Under other chamber configurations, as well as in the historical reference tests, the same sample achieved average capture efficiencies over seventy percent.

The major difference between chamber code A and all other experimental layouts is the position of the tracer emitter assembly being further into the room and farther from the range hood. In layout A, the electric burners and emitters are embedded in the simulated cooktop area beneath the range hood and are located such that the center of each emitter is 19.69 inches, or 500 mm, away from the back wall of the chamber. In chamber configurations B, C, and D this distance was reduced to 17.69 inches, or approximately 450 mm. Note that ASTM-E3087 specifies that this distance should be 500 mm ± 25 mm, meaning that chamber code A is the only one of the four tested layouts that complies with the standard. The substantial difference in results obtained in this study highlights the sensitivity of capture efficiency testing, especially at low operating speeds, to the location of the tracer gas emitters.

CHAPTER 8.

CONCLUSIONS

There are a variety of range hoods commercially available to maintain indoor air quality by removing contaminants released by cooking. The capture efficiency testing procedure set forth in ASTM-E3087 combines the effects of many of the parameters that might influence a hood's performance into a single percentage, referred to as capture efficiency (CE). This standard testing procedure is effective, but it can still be improved in the areas of test repeatability and automation potential. This thesis suggests two modified test methods that adapt most of the existing test framework except that an array of three different tracer gas concentration sensors replace the existing single-sensor approach. The first proposed method requires a technician to manually enter data at each point. The second proposed test method is automatic, and it only requires the technician to initialize a recording program, and then supervision to ensure stable conditions during the test.

First, the proposed multi-sensor test methods were validated by performing a series of tests on two sample range hoods that had been previously tested at REEL using the single-sensor method described in ASTM-E3087. Tests were performed at four operating speeds using each proposed method. The averaged results of these tests were compared to those gathered with the single-sensor method through a series of t-tests. These comparisons show that in all four test cases, both the manual and automatic multi-sensor methods produce statistically similar results to the single-sensor method for an assumed 95% confidence level. On average, results of the manual method differed from

single sensor results by only 1.502% and results of the automatic method differed by only 1.516%

After validation, the two multi-sensor methods were compared against each other to determine which is more repeatable. Five sample range hoods were used for comparison at a total of twelve operating conditions. Repeatability was assessed by comparing the standard deviation of results gathered for each operating condition. The manual method appears to be more repeatable than the automatic method, reporting an average standard deviation of 1.573% compared to 1.769% reported by the automatic method. The lower repeatability of the automatic results likely stems from the increased number of measurements taken with this method and the fact that it does not include any means of filtering out outlier measurements during a test.

Finally, the manual multi-sensor test method was used to perform an investigation into the impacts of chamber hardware layouts on measured capture efficiency results. In this test series, one range hood was tested at two operating speeds in a total of four different chamber layouts (i.e., test facility modifications made with the goal of simulating actual kitchen and cooking conditions). These experimental results were compared to a set of tests performed by REEL on the same sample. The results of this study emphasized the sensitivity of capture efficiency testing at low operating speeds and the significance of the distance between the tracer gas emitter assemblies and the back wall of the test chamber. Results of testing showed that when the emitters were moved just two inches further away from the back wall of the chamber, the average measured capture efficiency at low speed was 18% lower than the historical reference.

In all other chamber configurations, where this dimension matched that of the reference tests, the average measured capture efficiency at low speed differed from the reference data by 3.8% or less.

REFERENCES

1. *The benefit of kitchen exhaust fan use after cooking - An experimental assessment.* **Dobbin, Nina A., .** 2018, Building and Environment, Vol. 135, pp. 286-296.

2. **ASTM International.** Standard Test Method for Measuring Capture Efficiency of Domestic Range Hoods. *ASTM Standard E3087-18.* West Conshohocken, PA : ASTM International, 2018.

3. *The Design, Construction and Evaluation of a Test Chamber for Measuring Range Hood Capture Efficiency.* **Meleika, S., Hicks, T., Pate, M. and Sweeney, J.** 2020, Science and Technology for the Built Environment, Vol. 26, Issue 6, pp. 856-872.

4. **PP Systems Inc.** SBA-5 CO2 Analyzer Operation Manual. : PP Systems Inc., 2015.

5. **Siegle, Del.** t Test. *Educational Research Basics by Del Siegle* . [] University of Connecticut, May 22, 2015. researchbasics.education.uconn.edu/t-test.

6. **Zaiontz, Charles.** Two Sample t Test: Equal Variances. *Real Statistics Using Excel.* [] www.real-statistics.com/students-t-distribution/two-sample-t-test-equal-variances/.

7. *(2016) Development of a Tracer Gas Capture Efficiency Test Method for Residential Kitchen Ventilation.* **Walker, I.S., Sherman, M.H., Singer, B.C. and Delp, W.W.** 2016. Proc. IAQ.

8. *The Effects of Range Hood Mounting Height on Capture Efficiency.* **Meleika, S., Pate, M., and Jacquesson, A.** 2020 accepted (Published online 2021), Science and Technology for the Built Environment.

9. *The effects of cook-top temperature on range hood capture efficiency.* **Meleika, S. Pate, M.** (Published online 2020), 2021, Science and Technology for the Built Environment, Vol. 27, Issue 2, pp. 283-302.

10. **ASTM International.** ASTM E2029-11 (2019), Standard Test Method for Volumetric and Mass Flow Rate Measurement in a Duct Using Tracer Gas Dilution. West Conshohocken, PA : ASTM International, 2019.